CHAPTER III

A new cobalt(II) complex of 7-methylpterin-6-carboxylic acid with 1, 10- phenanthroline as the ancillary ligand: synthesis, x-ray structural, physico-chemical, kinetic studies and DFT calculations.

Abstract

A new mixed ligand cobalt(II) complex of the title ligands has been synthesized and characterized using elemental analysis, ESIMS and x-ray structural data as well as different physico-chemical studies. X-ray data of this compound [Co(L)(phen)(H_2O)].3H_2O reveals tridentate pterin coordination towards a mononuclear Co(II) atom. The neutral bidentate ancillary ligand [1, 10-phenanthroline (phen)] and the aqua group complete the distorted octahedron around the metal center. Near perpendicular disposition of the two chelate rings involving pterin and phen, respectively is indicated. The crystal forces are further augmented by two types of π-π stacking involving the pterin ring and phen. The cyclic voltamogram is characterized by several irreversible reduction peaks (-0.6, -1.1V, -1.3V and -1.6V respectively) of which the one at -0.6 V can be assigned to a metal-centered reduction process, e.g. Co (II) → Co(I). The group transfer reaction involving replacement of the aquo group of this complex by imidazole has been followed kinetically giving a k_{obs} value of $2.6x10^{-2}$ s^{-1} and $\Delta S^{\neq}$ = - 256.0 J $mol^{-1}deg^{-1}$ respectively; the negative $\Delta S^{\neq}$ value indicates an associative pathway. Reactivity of this Co(II) complex towards $NaBH_4$ as well as that of the $NaBH_4$ reduction product towards bromobenzene have been followed spectrophotometrically in presence of O_2; activation of the aromatic ring of bromobenzene towards hydroxylation could be inferred from the associated stoichiometric studies. Gaussian DFT calculations throw lights on the frontier orbital energies as well as their percentage compositions and help to rationalize the above reactivities.

Introduction

The most important biochemical role of cobalt is associated with vitamin B_{12}, which is the only vitamin known to contain a metal. Vitamin B_{12} is involved in a number of biochemical processes, the most important being the formation of red blood cells (erythrocytes). Reaction of vitamin B_{12} with ATP leads to the formation of vitamin B_{12}-coenzyme, which is involved in effecting many unusual rearrangement reactions.

Vitamin B_{12}, cobalamin (orange) can be reduced in two successive one electron steps into vitamin B_{12r} (brown) and vitamin $B_{12s,}$ with the cobalt centres existing in the +3, +2 and +1 oxidation states respectively.

$$\underset{\text{(orange)}}{B_{12}Co^{III} - X} \overset{e'}{\rightleftharpoons} \underset{\text{(brown)}}{B_{12r}Co^{II}} \overset{e'}{\rightleftharpoons} \underset{\text{(bluegreen)}}{B_{12s}Co^{I}}$$

In biological systems, these reductions are carried out by NADH and $FADH_2$. Reduced vitamin B_{12} species (the B_{12s}) is a powerful reducing agent which reduces ClO_3' to Cl' and at pH 1.5 – 2.5 NO_3' to NH_4^+. The vitamin B_{12s} (blue-green) species is also strongly nucleophilic and undergoes ready alkylation leading to the formation of a Co-C bond:

$$B_{12s}Co^{I} + MeI \rightarrow [B_{12}Co^{III}\text{-}Me]^+ + I'.$$

Cobalt is also biologically important in some enzymes. Glutamic mutase is involved in the metabolism of amino acids and ribonucleotide reductase in the biosynthesis of DNA.

In the light of the aims and objectives of this treatise, the coordination chemistry of the cobalt (II) ion (d^7) is explored here using the pterin ligand 7-methylpterin-6-carboxylic acid (H_2L). A couple factors have guided the choice of Co (II) for this work e. g. the avidity of Co (II) complexes for molecular oxygen as well as the ability of this d^7 system to balance the extent of M→L π bonding (with molecular oxygen) with the transmission of reducing property of the

pterin ligand to the reaction site, using bromobenzene as a model substrate for PAH activity. $NaBH_4$ is used here as the source of reducing equivalants.

Choice of 1, 10-phenanthroline (phen) as the ancillary ligand here depends solely on its ability to provide with x-ray quality crystals of the resulting Co (II) mixed ligand complex. 2, 2´-bipyridine (bipy) is unable to achieve this objective. Ability of such π-acid ligands to form Co(I) (d^8) complexes . e g. $[Co(bipy)_3]^+$ is well-known[79]. There is scope for accessing the Co(I) state chemically/electrochemically using the Co(II) complex. Gaussian DFT calculations on present system have been used to obtained information about the electronic structures which help to rationalize the reactivity aspects.

Experimental

Materials. Reagent grade chemicals were used as received. Solvents were purified, prior to use, following literature procedure [20]. $CoSO_4.\ 7H_2O$ was obtained from BDH, E. Merck, Mumbai. NaOH was obtained from SRL, Mumbai and 1, 10-phenanthroline was obtained from E. Merck, Mumbai. Kinetic and electrochemical measurements were performed in spectroscopic grade DMSO (SRL, Mumbai). Bu_4NClO_4 (TBAP) for CV measurements was obtained by published methods [72].

Methods. X-ray (Bruker Smart Apex CCD), elemental analysis (Elementor, Vario Micro Cube-C,H,N) and CD (Jasco J-815) data were obtained from the CSMCRI,Bhavnagar,Gujrat. The basic CD data were smoothened using the Origin Pro 8 software. The electrospray mass spectra in CH_3OH were obtained from RSIC, Lucknow (Agilent 6520 Q-TOF mass spectrometer).Room temperature magnetic moment data were obtained by using a Sherwood magnetic susceptibility balance (model MSB Mk1). IR spectra (KBr pellet) were recorded on a Perkin Elmer IR

spectrometer (model RX 1). Cyclic voltammetric experiments were performed with a Bioanalytical Systems Epsilon electrochemical workstation (model CV-50) using 1.0mM analyte in DMSO (0.1M TBAP; glassy carbon working electrode). Electronic spectra and kinetic data (under N_2- atmosphere) were recorded on a Jasco (UV–530) spectrophotometer, with thermostatic conditions (± 0.5 K) being maintained using a Shimadzu (TB–85) thermostat. Pseudo-first-order rate constants (k_{obs}, s^{-1}) were determined by the least square method from the plots of $\log(A_\infty - A_t)$ vs. time, which were linear for at least three half-lives. These rate constants measured at four different temparatures, were used to determine activation parameters by means of an Eyring plot [$\ln (k_{obs}/T)$ vs. $(1/T)$]. The frontier orbitals diagrams were obtained by Gaussian 09 and Gauss View 05 computer softwares.

Synthesis .

2-Amino-4-hydroxy-7-methylpteridine-6-carboxylic acid sesquihydrate ($C_8H_7N_5O_3$. $1.5H_2O$) (1)

The pterin ligand 2-amino-4-hydroxy-7-methylpteridine-6-carboxylic acid sesquihydrate ($C_8H_7N_5O_3$. $1.5H_2O$) was obtained by published procedure. (Wittle et.al., 1947)[19]. Ligand (**1**) was prepared in 75 % yield by modifying the original method of synthesis in the light of later developments (e.g., darkness, N_2 – atmosphere) [73]. The product decomposed without melting above 573 K. It is soluble in aqueous/methanolic NaOH/KOH and Bu_4NOH. Found : C, 44.0; H, 4.4; N, 28.4 %. Calc. for $C_8H_7N_5O_3$. $1.5H_2O$: C, 44.3; H, 4.1; N, 28.7 %. UV – VIS absorption bands [NaOH, $\lambda_{max}^{nm}(\log\epsilon)$]: 293 (3.68), 341 (3.86), 400 (3.28), 422 (3.27), 456 sh (3.00).

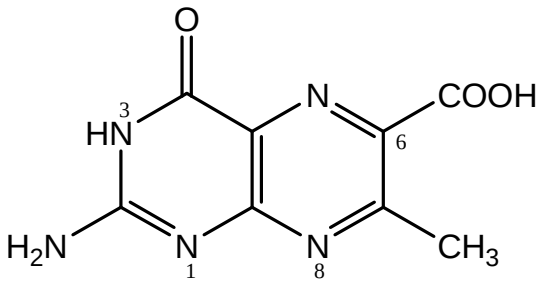

The pterin ligand (H_2L)

Scheme III-1

[Co($C_8H_5N_5O_3$)($C_{12}H_8N_2$)(H_2O)]. $3H_2O$ (2)

The title complex was prepared by the dropwise addition of an aqueous alkaline solution (NaOH : 11 mg, 0.275mmol) of the pterin ligand (35 mg, 0.125 mmol) to a warm (311K) aqueous reaction medium containing $CoSO_4$. $7H_2O$ (35 mg, 0.125 mmol) and 1, 10-phenanthroline monohydrate (25 mg, 0.125 mmol) in a total volume of 60 ml. The pH value was adjusted to 10.8 using aqueous NaOH solution and dioxygen was bubbled in for 48h; final pH was 10.3. Initially a small amount of yellow-white precipitate came out and the reaction mixture ultimately assumed as a reddish-pink tinge. It was transferred to a 100 ml beaker, requisite quantity of water was added to make up for the evaporation loss and allowed to stand at room temperature. Pink crystals suitable for single crystal x-ray diffraction appeared after 15 days (yield : 30%). Found: C, 43.0; H, 3.69; N, 17.81%. Calc. for [Co($C_8H_5N_5O_3$)($C_{12}H_8N_2$)(H_2O)] $3H_2O$,: C, 45.25; H, 3.96; N, 18.47%. UV-VIS absorption bands [CH_3OH, λ_{max}nm (logε)]: 268(4.35), 372(3.65), 540br(2.22), 620br(2.19), 678(2.20), 712sh(2.17), 744(2.18), 807(2.18), 924sh(2.00), 970sh(1.9), 1056br(1.83)

$CoSO_4.\ 7H_2O$ + 1, 10- phenanthroline + H_2L(aq NaOH) $\xrightarrow{O_2,\ 38^0C,\ 48h}$ $[Co(L)(phen)(H_2O)].\ 3H_2O$

Scheme III-2

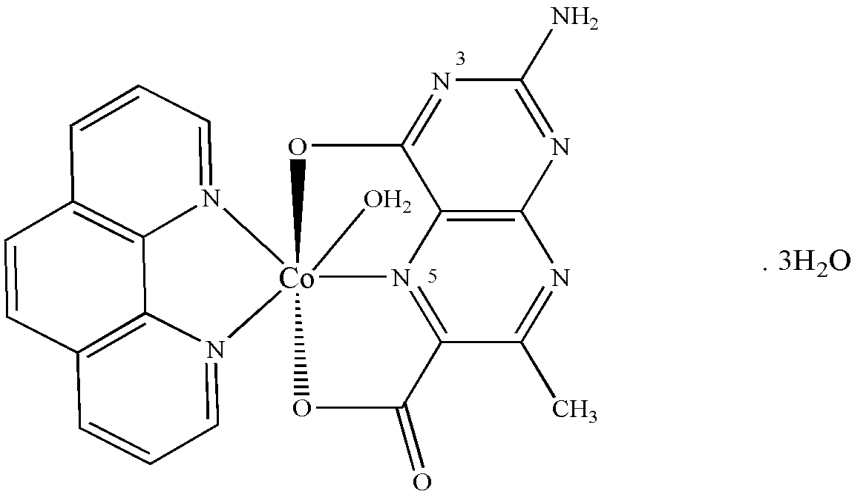

$.\ 3H_2O$

Scheme III-3 (compound **2**)

$Na[Co^I(L')(phen)\ (H_2O)].\ 2H_2O.CH_3OH$ (3)

Synthesis of $Na[Co^I(L')(phen)\ (H_2O)].\ 2H_2O.CH_3OH$ (**3**), where $(L')^{2-}$ is the 7,8-dihydro form (Scheme II-4) of the pterin ligand anion (Scheme II-1), as established on the basis of microanalytical and spectroscopic data (vide infra). A methanolic solution (50 mL) of **2** (26.51 mg, 0.05 mmol) was treated with $NaBH_4$ (11.3 mg, 0.3 mmol) and the reaction was allowed to continue for 45 min at 301-303K under subdued light in a Schlenk flask attached to a paraffin oil bubbler. The reaction mixture passed through a sequence of color changes e.g., bright orange → snuff colour . It was then rotavapped and a dark brown solid was recovered (Scheme II-6). It was washed quickly (decantation) with dinitrogen purged CH_3OH (3 X 4 mL) and dried in vacuo

over silica gel for 48h.Yield: 35%. Anal. Calcd for $NaCoC_{21}H_{25}N_7O_7$: C, 44.29; H, 4.39; N, 17.22. Found: C,43.24; H, 3.89; N, 17.58.

Results and Discussion

Synthesis of the present Co(II) mixed ligand complex (**2**) is not straight forward. Initially a small quantity of yellow-white precipitate of unknown composition came out and only after prolonged exposer to dioxygen at 38^0C, it could be redissolved and the desired crystals could be obtained. The crystals have to be dried in vacuo for at least 48 hours for getting analytically pure samples, suitable for elemental analysis (C-H-N) and mass spectral data (ESIMS).

The elegance of the synthetic procedure is that the complex compound of a pterin ligand could be crystallized out of the aqueous medium, whereas pterin compounds usually suffers from low solubility problems[74]. Most likely the presence of hydrophilic groups like – COOH and – OH in the pterin ligand contributes to the enhanced solubility of (**2**) in aqueous alkaline medium (ca. pH ≈ 10.5).

Molcular Structure of $[Co(C_8H_5N_5O_3)(C_{12}H_8N_2)(H_2O)].\ 3H_2O$ (2). In the title compound (**2**) (Figure III-1), the stereochemistry around the Co(II) atom is essentially distorted octahedral with two N atoms of phen, a pyrazine ring N atom (N3) of the pterin ligand and an aqua O atom forming the equatorial plane; two pterin O atoms (O1 and O3) define the longer axial positions, with the phenolate O3 forming the longest axial bond [2.270 (2) Å]. Extent of distortion of this coordination octahedron is much more pronounced as compared to that of the Co(II)-pteridine complexes reported earlier (Acuna-Cueva *et al.*, 2003; Burgmayer & Stiefel, 1988; Funahashi *et al.*,1997)[15,25,76]. A major cause of this departure from regular geometry is that the pterin ligand forms two five-membered chelate rings having small bite angles [75.10 (10) and 76.26 (9)°], instead of only one per pteridine ligand for the earlier cases. Location of the short

Co1—N3 bond [2.016 (3) Å] in the equatorial plane is consistent with the literature, which suggests a strong cobalt-pterin interaction (Odani *et al.*, 1992)[18c]. The pterin ligand is coordinated here as a binegative tridentate ONO donor, as evident from the charge balance of this complex. The phen and pterin rings are nearly perpendicular to each other for minimizing the steric repulsion. The Co1—N1 [2.079 (3) Å] and Co1—N2 [2.123 (3) Å] bond lengths are at par with that of the Co1—N3 bond [2.016 (3) Å] and indicate receipt of π-back donation to both phen and pterin rings from the Co(II) centre (d^7) through $d\pi$–$p\pi$ interactions. This process is further strengthened by the presence of π-donating phenolate and carboxylate O atoms around the metal centre (Kohzuma *et al.*, 1988)[18a]. For rationalizing the near double bond nature of the O3—C18 [1.265 (4) Å] bond, a hypothesis of Joule (Scheme III-4) (Beddoes *et al.*, 1993; Russell *et al.*, 1992)[22,23] may be invoked, which suggests withdrawl of electron density from the pyrazine ring N6 by the pyrimidine ring C18-carbonyl group through mesomeric interaction. Formation of the O3—Co1 bond accentuates this electron withdrawal towards O3. The electron-rich N7—C17 [1.337 (4) Å] bond may also participate in this electron transfer (Figure III-1). The presence of hydrogen-bonded electron transfer proteins (iron-sulphur proteins) at the pterin ring NH_2(2) position (Scheme III-1, III-2 , III-4) as revealed by x-ray crystallography for oxomolybdoenzymes, may bear instructive relation with the above-mentioned electron transfer process from N7 to O3 (bonded to the metal centre)[10] .The pyrimidine ring is fairly planar and deviations of the C16/N5/C17 and C17/N4/C18 segments with respect to the N7—C17 multiple bonds are 2.6 and 0.7°, respectively. The crystal data and geometric parameters of (**2**) are shown in Tables (III-1) and (III-2) respectively.

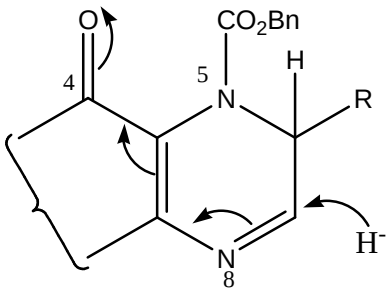

Scheme III-4

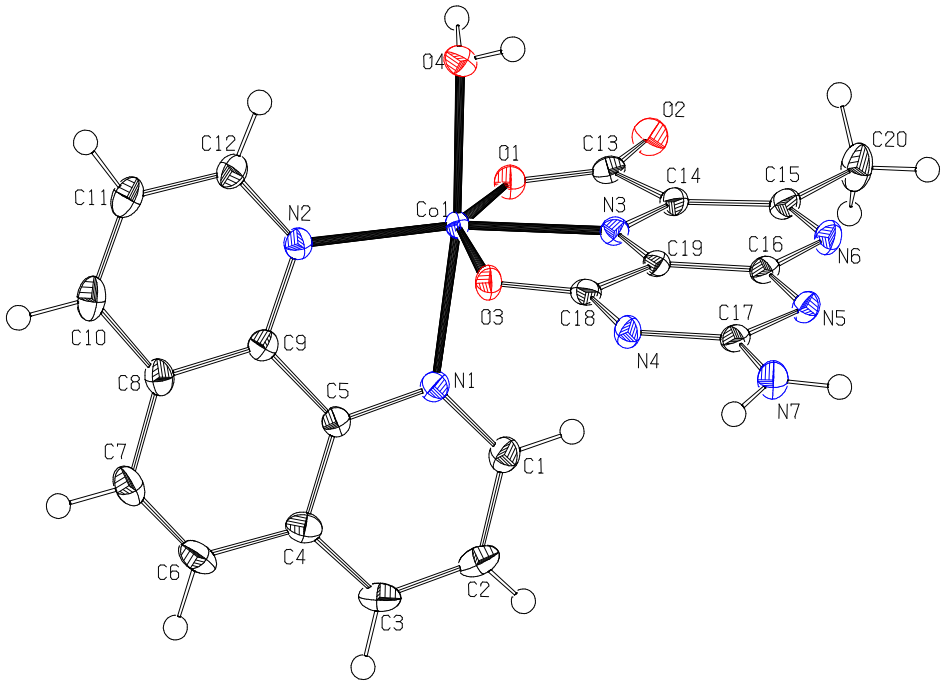

Figure III- 1 ORTEP diagram of (**2**) with atom numbering scheme (50% probability factor for the thermal ellipsoids). Lattice water molecules are omitted for clarity.

Table III-1. Crystal data and structure refinement for (2).

Identification code	**2**
Empirical formula	$C_{20}H_{21}CoN_7O_7$
Formula weight	530.36
Temperature/K	110
Crystal system	Triclinic
Space group	P-1
a/Å	8.454(2)
b/Å	9.934(3)
c/Å	13.778(4)
α/°	97.534(4)
β/°	95.281(4)
γ/°	110.603(4)
Volume/Å^3	1061.8(5)
Z	2
ρ_{calc}g/cm^3	1.659
μ/mm^{-1}	0.870
F(000)	546.0
Crystal size/mm^3	0.230 × 0.110 × 0.040
Radiation	Mo Kα (λ = 0.71073)
2Θ range for data collection/°	3.016 to 56.398

Index ranges	$-11 \leq h \leq 11, -12 \leq k \leq 13, -18 \leq l \leq 18$
Reflections collected	8945
Independent reflections	4744 [$R_{int} = 0.030$, $R_{sigma} = 0.665$]
Data/restraints/parameters	4744/0/316
Goodness-of-fit on F^2	1.029
Final R indexes [I>=2σ (I)]	$R_1 = 0.0567$, $wR_2 = 0.1257$
Final R indexes [all data]	$R_1 = 0.0626$, $wR_2 = 0.1290$
Largest diff. peak/hole / e $Å^{-3}$	0.99/-0.88

Table III-2. Geometric parameters of (2)

Atoms 1,2	d 1,2 [Å]	Atoms 1,2	d 1,2 [Å]
Co1—O1	2.140(2)	N2—C12	1.333(4)
Co1—N3	2.016(3)	N2—C9	1.355(4)
Co1—O3	2.270(2)	C12—C11	1.402(5)
Co1—O4	2.120(2)	C12—H12	0.9230
Co1—N2	2.123(3)	C11—C10	1.363(5)
Co1—N1	2.079(3)	C11—H11	0.9140
O1—C13	1.279(4)	C10—C8	1.414(5)
C13—O2	1.244(4)	C10—H10	0.9260
C13—C14	1.519(4)	C8—C9	1.408(4)
C14—N3	1.319(4)	C8—C7	1.435(5)

C14—C15	1.426(4)	C9—C5	1.439(4)
N3—C19	1.319(4)	C5—N1	1.359(4)
C19—C16	1.397(4)	C5—C4	1.411(4)
C19—C18	1.450(4)	N1—C1	1.333(4)
C16—N5	1.354(4)	C1—C2	1.406(5)
C16—N6	1.360(4)	C1—H1	0.9300
N5—C17	1.360(4)	C2—C3	1.363(5)
C17—N4	1.378(4)	C2—H2	0.9280
C17—N7	1.337(4)	C3—C4	1.412(5)
N4—C18	1.335(4)	C3—H3	0.9280
C18—O3	1.265(4)	C4—C6	1.439(5)
N7—H7a	0.8520	C6—C7	1.349(5)
N7—H7b	0.8430	C6—H6	0.9250
N6—C15	1.342(4)	C7—H7	0.9260
C15—C20	1.491(4)	O7—H7c	0.8010
C20—H20a	0.9470	O7—H7d	0.8090
C20—H20b	0.9600	O5—H5a	0.8180
C20—H20c	0.9300	O5—H5b	0.8170
O4—H4a	0.8100	O6—H6a	0.8250
O4—H4b	0.8010	O6—H6b	0.8180

Atoms 1,2,3	Angle 1,2,3 [°]	Atoms 1,2,3	Angle 1,2,3 [°]

O1—Co1—N3	75.1(1)	H20a—C20—H20c	106.600
O1—Co1—O3	151.22(8)	H20b—C20—H20c	109.700
O1—Co1—O4	90.13(9)	Co1—O4—H4a	116.600
O1—Co1—N2	90.99(10)	Co1—O4—H4b	109.700
O1—Co1—N1	119.55(10)	H4a—O4—H4b	95.300
N3—Co1—O3	76.26(9)	Co1—N2—C12	128.8(2)
N3—Co1—O4	90.23(10)	Co1—N2—C9	112.7(2)
N3—Co1—N2	96.45(10)	C12—N2—C9	118.5(3)
N3—Co1—N1	164.48(10)	N2—C12—C11	122.3(3)
O3—Co1—O4	92.74(9)	N2—C12—H12	119.100
O3—Co1—N2	89.46(9)	C11—C12—H12	118.600
O3—Co1—N1	88.76(9)	C12—C11—C10	119.6(3)
O4—Co1—N2	173.29(10)	C12—C11—H11	120.200
O4—Co1—N1	94.58(10)	C10—C11—H11	120.200
N2—Co1—N1	79.12(10)	C11—C10—C8	119.9(3)
Co1—O1—C13	116.8(2)	C11—C10—H10	120.100
O1—C13—O2	124.1(3)	C8—C10—H10	120.000
O1—C13—C14	114.6(3)	C10—C8—C9	116.7(3)
O2—C13—C14	121.2(3)	C10—C8—C7	124.4(3)
C13—C14—N3	111.4(3)	C9—C8—C7	118.9(3)
C13—C14—C15	129.9(3)	N2—C9—C5	116.8(3)
N3—C14—C15	118.8(3)	C8—C9—N2	123.1(3)

Co1—N3—C14	121.6(2)	C8—C9—C5	120.1(3)
Co1—N3—C19	117.6(2)	C9—C5—N1	117.5(3)
C14—N3—C19	120.8(3)	C9—C5—C4	119.5(3)
N3—C19—C16	121.8(3)	N1—C5—C4	123.0(3)
N3—C19—C18	117.4(3)	Co1—N1—C5	113.6(2)
C16—C19—C18	120.7(3)	Co1—N1—C1	127.6(2)
C19—C16—N5	120.8(3)	C5—N1—C1	118.5(3)
C19—C16—N6	118.7(3)	N1—C1—C2	122.0(3)
N5—C16—N6	120.4(3)	N1—C1—H1	118.000
C16—N5—C17	115.1(3)	C2—C1—H1	120.000
N5—C17—N4	127.9(3)	C1—C2—C3	119.8(3)
N5—C17—N7	117.0(3)	C1—C2—H2	119.300
N4—C17—N7	115.1(3)	C3—C2—H2	120.900
C17—N4—C18	117.6(3)	C2—C3—C4	119.9(3)
C19—C18—N4	117.7(3)	C2—C3—H3	120.700
C19—C18—O3	118.1(3)	C4—C3—H3	119.400
N4—C18—O3	124.2(3)	C5—C4—C6	119.0(3)
Co1—O3—C18	110.63(19)	C3—C4—C5	116.8(3)
C17—N7—H7a	119.800	C3—C4—C6	124.2(3)
C17—N7—H7b	119.900	C4—C6—C7	121.2(3)
H7a—N7—H7b	117.600	C4—C6—H6	119.500
C16—N6—C15	119.0(3)	C7—C6—H6	119.200

C14—C15—N6	120.8(3)	C8—C7—C6	121.3(3)
C14—C15—C20	121.7(3)	C8—C7—H7	118.400
N6—C15—C20	117.4(3)	C6—C7—H7	120.300
C15—C20—H20a	111.500	H7c—O7—H7d	86.200
C15—C20—H20b	110.100	H5a—O5—H5b	108.700
C15—C20—H20c	110.700	H6a—O6—H6b	105.500
H20a—C20—H20b	108.200		

In the crystal, intermolecular N—H・・・O, O—H・・・N and O—H・・・O hydrogen bonds link the complex molecules and lattice water molecules into a layer parallel to (001) (Figure III-2). The lattice water molecules are decisive for the crystal packing. Table (III-3) shows a few hydrogen bond data. Figure III-3 reveals π–π stacking interactions involving two parallel, inversion-related pterin rings within the same unit cell and showing face-to-face distance of 3.283 (4) and 3.366 (4) Å. Again the phen rings display two types of π–π stacking on either side of the unit cell. In one case, the adjacent phen rings are essentially parallel to each other with an average interplanar distance of 3.496 (4) Å; on the other side of the unit cell, the face-to-face separations between parallel phen rings are 3.578 (4) and 3.629 (5) Å.

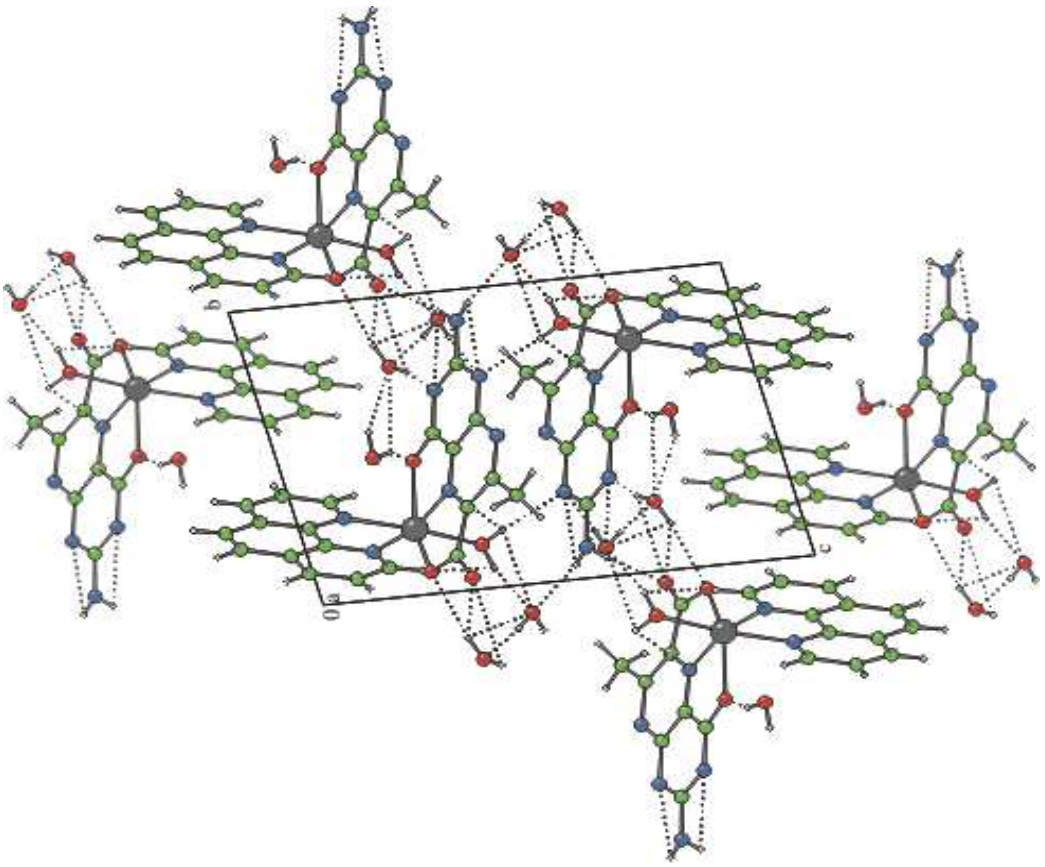

Figure III-2. The crystal packing diagram of (**2**), viewed along the *a* axis. Dotted lines indicate hydrogen bonds.

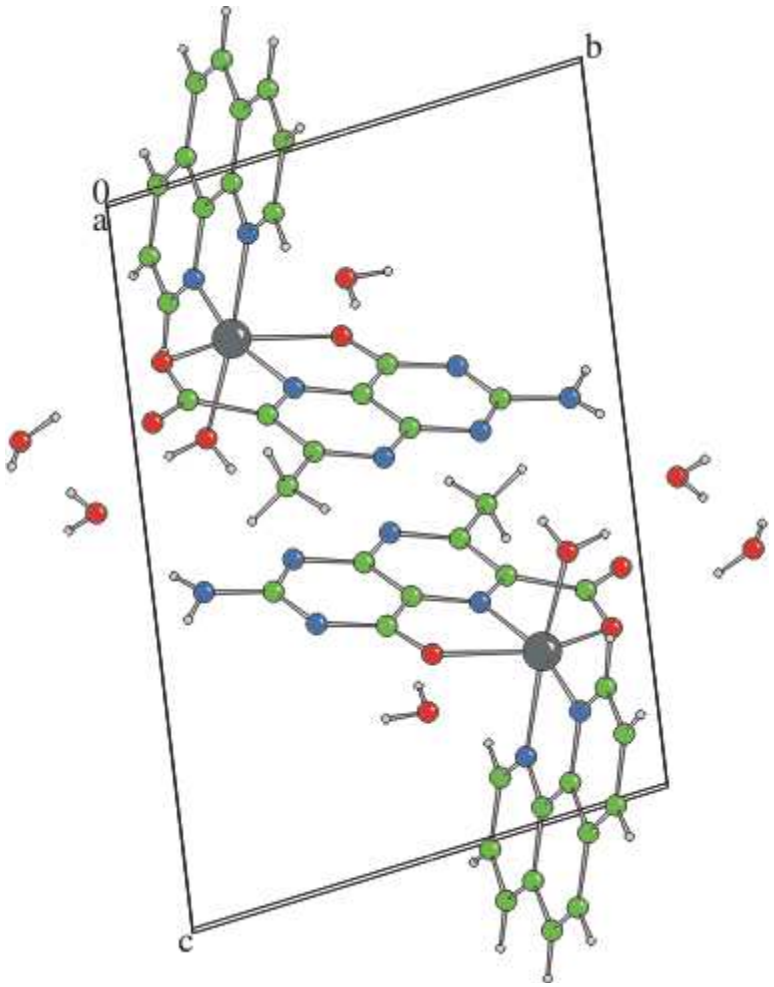

Figure III- 3. A molecular packing diagram highlighting π–π stacking interactions between two neighboring pterin–pterin rings of (**2**).

Table III-3. Selected hydrogen bonds of 2

Atoms D,H,A	Dist. D,H [Å]	Dist. H,A [Å]	Dist. D,A [Å]	Angle D,H,A [°]
N7—H7a—O2^{i}	0.8520	2.1150	2.941(5)	163.12(10)
N7—H7b—O6^{ii}	0.8430	2.1480	2.970(5)	164.91(10)
O4—H4a—O6	0.8100	1.9290	2.717(5)	164.33(10)
O4—H4b—N5^{ii}	0.8010	2.2510	3.050(5)	176.15(9)
O5—H5a—O1	0.8180	2.3390	3.079(5)	150.86(8)
O5—H5a—O2	0.8180	2.2320	2.896(5)	138.60(9)
O5—H5b—N4^{vi}	0.8170	2.0430	2.843(5)	166.42(10)
O6—H6a—O5	0.8250	1.9180	2.740(5)	174.33(10)
O6—H6b—N5^{vii}	0.8180	2.0530	2.870(5)	176.04(10)

(i) 1+x, 1+y, z; (ii) 1-x, 1-y, 1-z; (iii) 1+x, y, z; (iv) 1-x, 1-y, -z;

(v) -1+x, y, z; (vi) -1+x, -1+y, z; (vii) x, -1+y, z.

Mass spectrometry

Electrospray Ionization Mass Spectroscopy (ESIMS) involving soft ionization technique, has proved to be a valuable tool for characterizing wide variety of compounds including inorganic and coordination types [21,77,78]. This technique helps in assigning the molecular mass of this type of synthetic compounds. As true for different types of mass spectrometry, the assignment of

molecular formula (or any definite fragment originating from it) is confirmed by the experimental value of m/z (most abundant isotopic mass) as well as matching between the experimental and calculated (simulated) isotopic distribution profile [24]. As far as organic compounds containing O, F, P and I are concerned, the relative intensities of M, M+1 and M+2 isotope peaks are of great value in recognizing the molecular ion (M^+) peak or any well-defined fragment containing it [21]. For **1** a peak at m/z 222 (rel. inten.15%) corresponds to the dehydrated species $[M - 1.5H_2O + H]^+$ where $M(C_8H_7N_5O_3. 1.5H_2O)$ is the relevant molecular formula; the associated isotope pattern could be calculated[21,24]

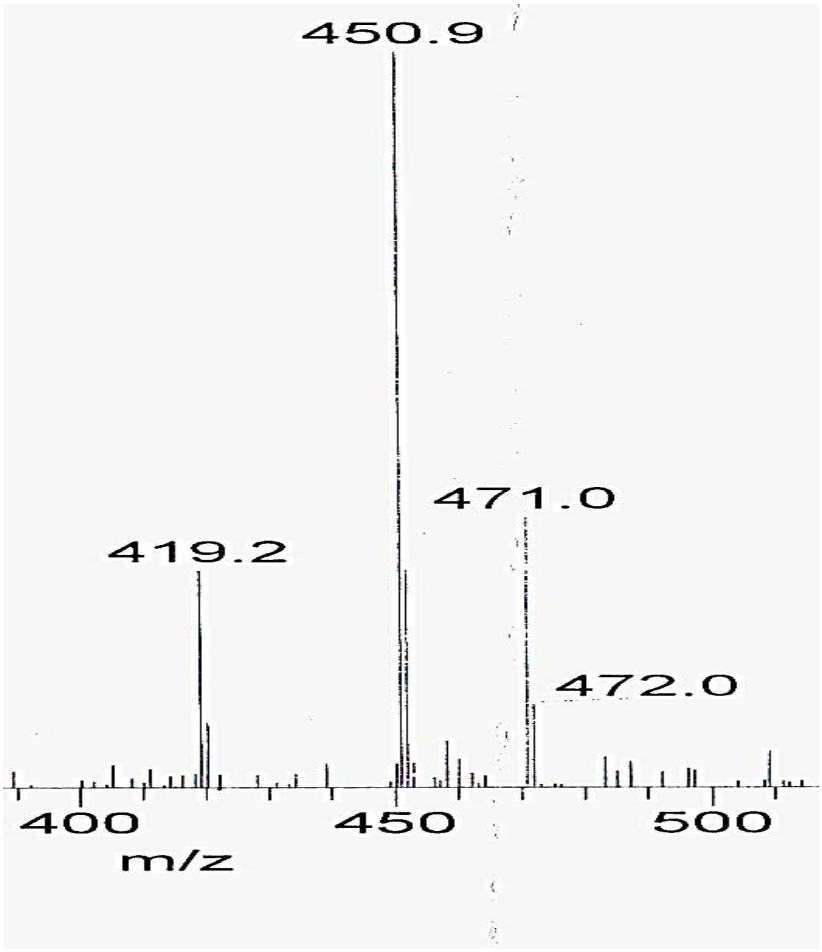

Figure III-4(a). ESIMS data of (**2**)

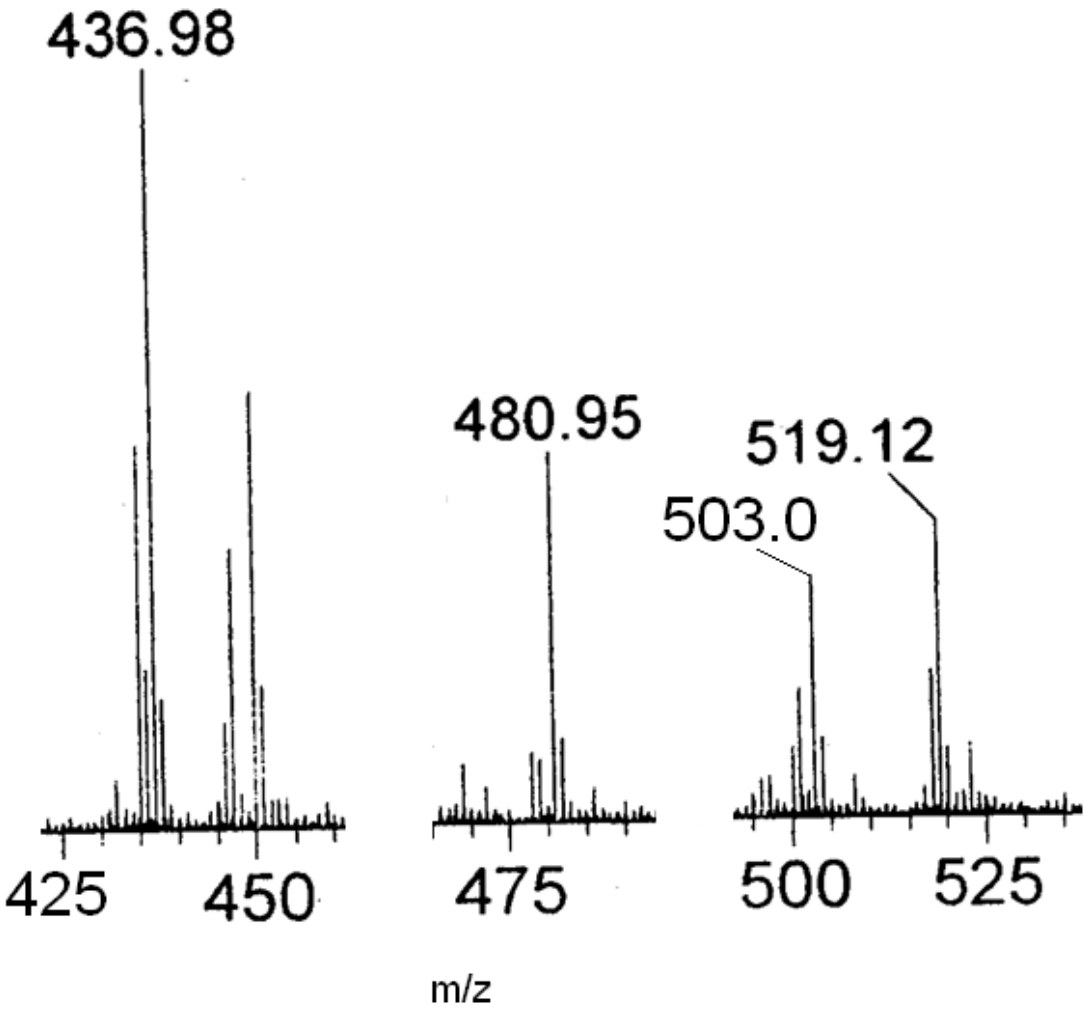

Figure III-4(b). ESIMS data of (**3**)

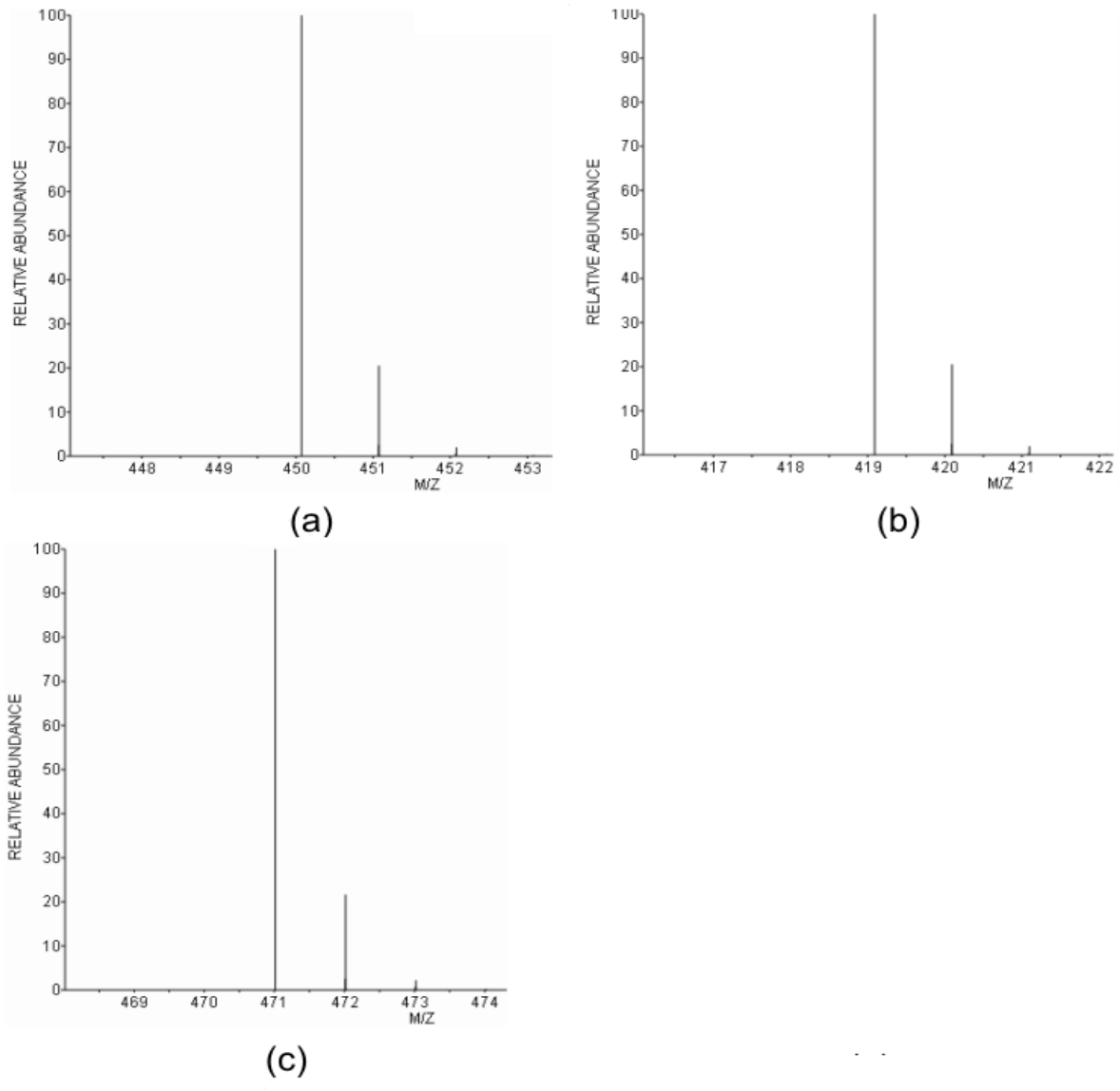

Figure III-5. The calculated isotope patterns for (**2**) ; (a) the base peak at m/z = 450.9 corresponding to the fragment $[M - 3H_2O - CO+2H]^+$, where M is the molecular formula of **2**; (b) and (c) correspond to the fragments $[M-4H_2O-CO_2+ 5H]^+$ and $[M-3H_2O-4H]^+$ respectively.

ESIMS data of **2** help to assign a few important fragments through comparison of experimental and simulated isotope distribution patterns. For example, the fragment $[M-3H_2O-4H]^+$ at

m/z=471.0 indicates removal of the extra spheric water molecules (Figure III-4a). The base peak at m/z = 450.0 can be assigned to the fragment $[M-3H_2O-CO+2H]^+$. Finally, the completely dehydrated species $[M-4H_2O-CO_2+5H]^+$ could be observed at m/z = 419.2. All these assignments could be verified through simulation experiments as indicated in Figure III-5. The fragments involving the gain or loss of 4 or 5 H atoms may apparently look unusual for molecular ion peaks, but they are justified for fragment ion peaks[21]. Sometimes, isotope peaks may be more instance than the calculated value because of ion-molecule interactions that vary with the sample concentration or with the class of compound involved e.g., the transfer of a hydrogen atom from the excess of the compound to the molecular ion in some cases[21].

The ESIMS data of **3** is shown in Figure III-4b. The peaks at m/z 519.12 ,m/z 503 and m/z 480.95 correspond to the fragmants $[M-CH_3OH - H_2O]^+$, $[M-CH_3OH -2H_2O]^+$ and $[M-CH_3OH -3H_2O - 2H]^+$, respectively, where M is the molecular formula of **3**. These peaks arise as a result of the stepwise loss of solvent molecules from the parent compound with the complex core remaining essentially intact. This aspect verifies the architectural stability of the coordination sphere around the Co(I) centre with the reduced pterin ligand (L'^{2-}, Scheme II-4).

Besides this, the peak at m/z 436.98 can be correlated with the fragmant $[M-CH_3OH - 3H_2O - CO_2 - 2H]^+$. Most of the isotopic distribution patterns can be simulated.

Magnetic susceptibility data of 2 and 3

Compound **2** shows an effective magnetic moment of 4.41BM at room temperature. For a high spin octahedral configuration of this Co(II) complex, the spin-only formula gives a moment of 3.88BM, corresponding to three unpaired electrons. Due to the intrinsic orbital angular

momentum in the octahedral ground state ($^4F/^4T_{1g}$), there is a considerable orbital contribution, leading to the observed higher value of the effective magnetic moment.[31,79] As discussed in the experimental section that **2** can be reduced with $NaBH_4$ in CH_3OH medium to a snuff coloured compound, isolated in the solid state and characterized to be **3**. Magnetic susceptibility data of this snuff coloured, non hygroscopic compound (**3**) was measured at room temperature (297K) and found to be 3.42BM. Spin-only formula predicts a μ_{eff} value of 2.83BM for two unpaired electrons. The above experimental μ_{eff} value is compatible with a high-spin Co(I) state (d^8, ^3F ground state) with substantial orbital contribution.[31] As evident from ^1H NMR data of **3** in chapter II, the $NaBH_4$ reduction process affords a 7,8-dihydro form of the pterin ligand residue ($L^2 \rightarrow L'^{2-}$)(Scheme II-4). As a logical extension of this idea to the present system **3,** it can be inferred that an uncommon oxidation state of cobalt, e.g, Co(I) could be stabilized here in an environment of such a reduced pterin ligand and a π-acid ligand (phen). X-ray structural data could verify in another pterin system that the pyrazine ring (pterin) is the reaction locant of $NaBH_4$ reduction.[22,23] Report exists about a tris Co(I) complex of 2, 2′-bipyridine, that is, enhanced stability of the low oxidation state of cobalt in presence of a π-acid ligand.[79] In other words, $NaBH_4$ is a suitable reducing agent for achieving both metal-centred [Co(II) → Co(I)] and pterin-centred [oxidized/aromatic state → 7, 8-dihydro state] reductions of **2**; the resulting reduced compound (**3**) is of sufficient stability for isolation in the solid state and magnetic susceptibility measurement. The thermodynamic favorability ($\Delta G^0 = -nFE^0$) of $NaBH_4$ reduction is indicated below. Cyclic voltametriy data of **2** indicates an E°′ value of -0.6 v for the Co(II) → Co(I) reduction; now using an E°′ value of -0.75V for $NaBH_4$ in neutral medium,[56-58] an E_{cell} value[$E_{cell} = E_1 - E_2 = -0.6 - (-0.75)$] 0.15 is obtained which is associated with a free energy

change [ΔG°] of 4.6 kcal mol^{-1}. This is consistent with relevant Frost diagram, indicating a small free energy change for the Co(II) → Co(I) reduction.

A simultaneous pterin-centred reduction is also achieved. The reverse step, that is, the oxidation of **3** with a mixture of bromobenzene/O_2 mixture, as discussed later, will highlight the functional modeling aspect for PAH activity associated with small free energy barriers for such conversions.

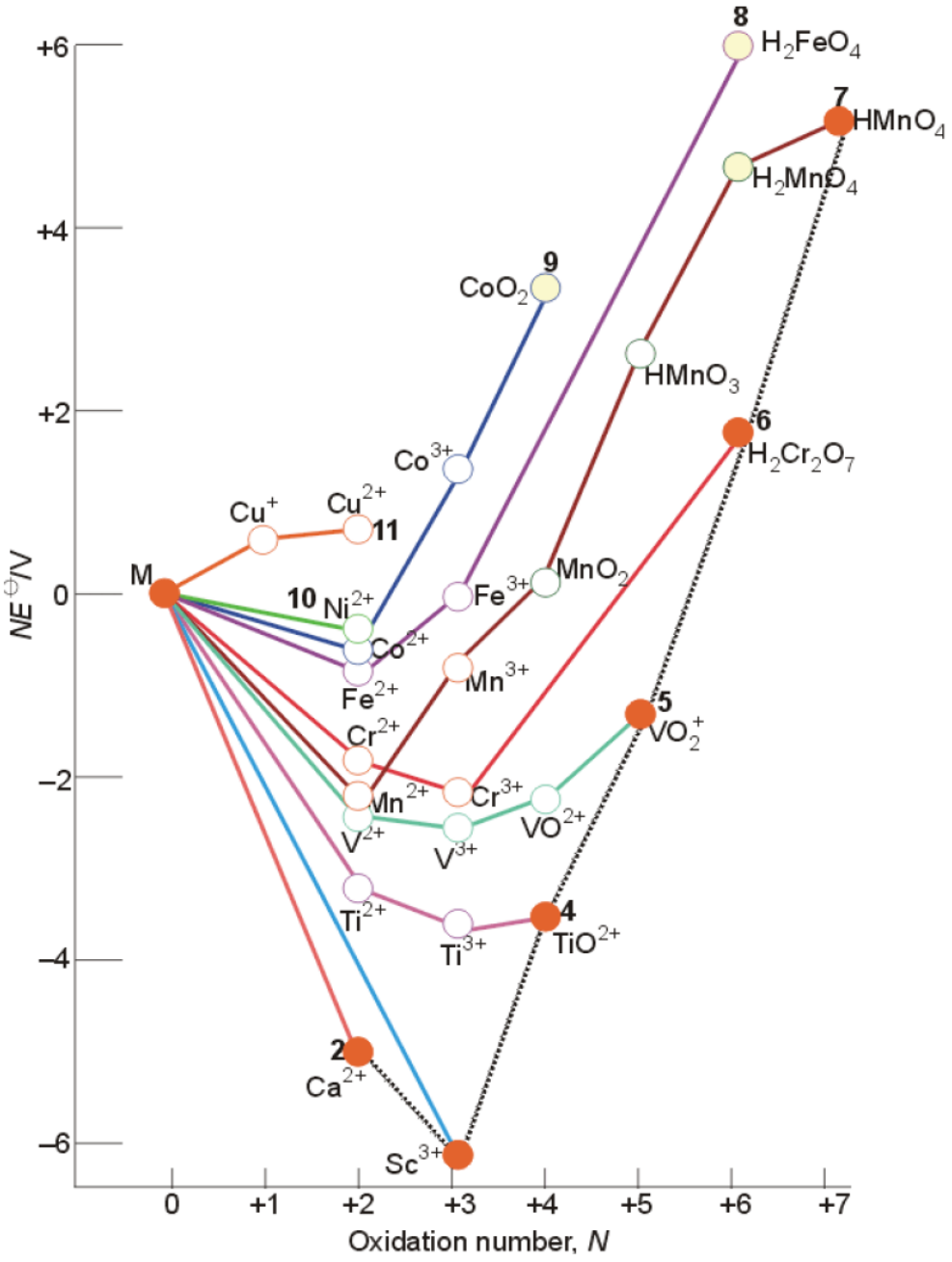

A Frost diagram for the first series of d-block elements in acidic solution(pH = 0). The broken line connects species in their group oxidation states.

IR Spectroscopy

The IR spectra (KBr pellets) of **1** and **2** are shown in Figure III-6 and III-7 respectively. For **1**, the free pterin ligand (Scheme III-1; Figure III-6) an intense broad band over the region 3250 – 3050 cm^{-1} corresponds to the ν(OH) and ν(NH) stretching vibrations of the hydrogen bonded lattice water molecules, the – COOH(6), NH(3) and NH_2(2) groups. The ν(C-H) stretching vibrations of the CH_3(7) group appear at 2851 cm^{-1} and 2757 cm^{-1} respectivly.[21] An intense broad band centered around 1684 cm^{-1} and extending over the region 1718 to 1636 cm^{-1}, characterizes the ν(C=O) modes of the C=O(4) group as well as that of the COOH(6) group (Scheme III-1). Some of the ν(C=C) and ν(C=N) modes of pterin ring could be identified around 1560-1539 cm^{-1}.[25,28] Two broad bands at 1383 cm^{-1} and 1294 cm^{-1} characterize the δ(O-H) and ν(C-O) + δ(O-H) modes respectively, of the –COOH group.[21] A series of bands observed over the region 860-650 cm^{-1}, are assigned to skeletal vibration of the pterin ligand. A prominent peak at 567 cm^{-1}, is assigned to rocking vibration of the NH_2(2) group.

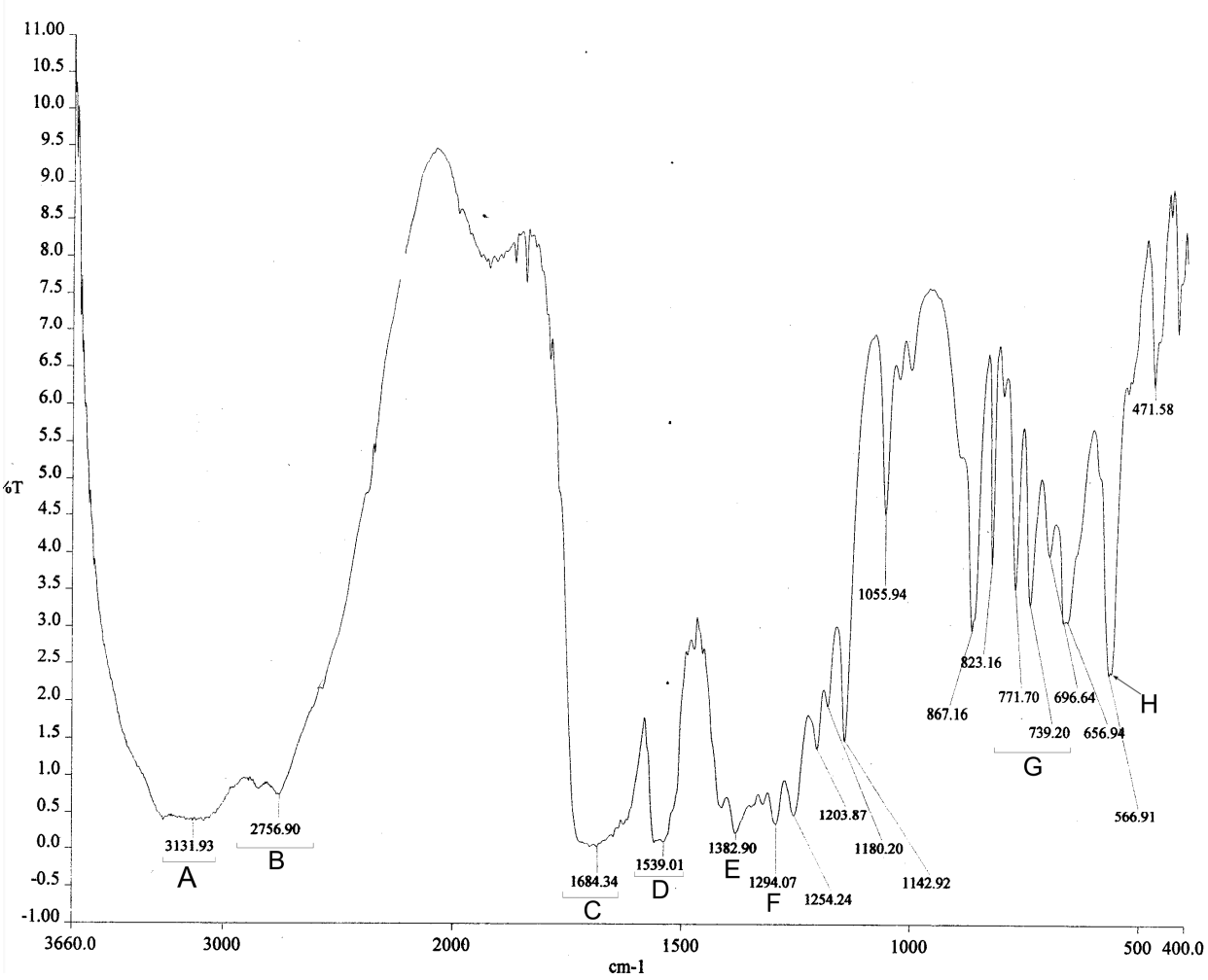

Figure III-6: FTIR spectrum (KBr) of the pterin ligand (H_2L)(**1**).

A: the broad band over the region 3250-3050 cm^{-1} due to the ν(OH) and ν(NH) stretching vibrations of the hydrogen bonded H_2O, - COOH(6), NH(3) and NH_2(2) groups , Scheme III-1;

B: the ν(CH) stretching vibrations of the CH_3(7) group are observed at 2851 cm^{-1} and 2757 cm^{-1} respectively;

C: an intense broad band centred at 1684 cm^{-1} and spread over the region 1718-1636 cm^{-1} is due to the ν(C=O) modes of the C=O(4) and COOH(6) groups, (Scheme III-1); the N-H bending vibrations at the NH_2(2) group are occluded under this band;

D: the ν(C=C) and ν(C=N) modes at the pterin ring appears around 1560-1539 cm^{-1};

E&F: the δ(O-H) and ν(C-O) + δ(O-H) modes of the COOH(6) group appear at 1382 cm^{-1} and 1294 cm^{-1} respectively;

G: different types of skeletal bending vibrations of the pterin ring appear over the region 860-650 cm^{-1};

H: rocking vibrations of the NH_2(2) group appears around 567 cm^{-1}.

Most of these assignments could be checked theoretically by simulating the IR spectrum of **1** using Gaussian 09 software program and viewing the result with the help of Gauss view 5.0

Figure III-7 shows the IR spectrum (KBr) of the cobalt complex **2**. Most of the above-mentioned broad IR bands of **1** (Figure III-6) undergo considerable modification through complex formation with the Co(II) ion, as evident from a comparative study of Figure III-6 and III-7 respectively. For **2** (Figure III-7) the ν(O-H) and ν(N-H) modes of H_2O molecule and NH_2(2) group appear at 3404 and 3338 cm^{-1} respectively. The ν(C-H) modes of phen moiety appear at 3209 and 3066 cm^{-1} respectively. The ν_{as} and ν_s stretching vibrations of the carboxylate group (6) appear at 1594.8 and 1369.7 cm^{-1} respectively.[21] The Δν value ($\nu_{as} - \nu_s$) of 224 cm^{-1} is consistent with monodentate carboxylate coordination.[87,88] The ν(C-O) mode of the coordinated (keto-enol tautomerism and deprotonation) C=O(4) group (pterin) appears at 1296.5 cm^{-1}. The

vibrations of the pterin ring are observed over the region 1518 – 1426 cm^{-1}.[25-28] The out-of-plane bending vibrations of the phen moiety (at 850 and 727 cm^{-1}) are also observed.[21]

Such data are consistent with tridentate pterin coordination involving the O(4), N(5) and CO_2^- (6) functional groups (Scheme III-1 and III-3) and supplement the x-ray structural data presented earlier (Figure III-1).

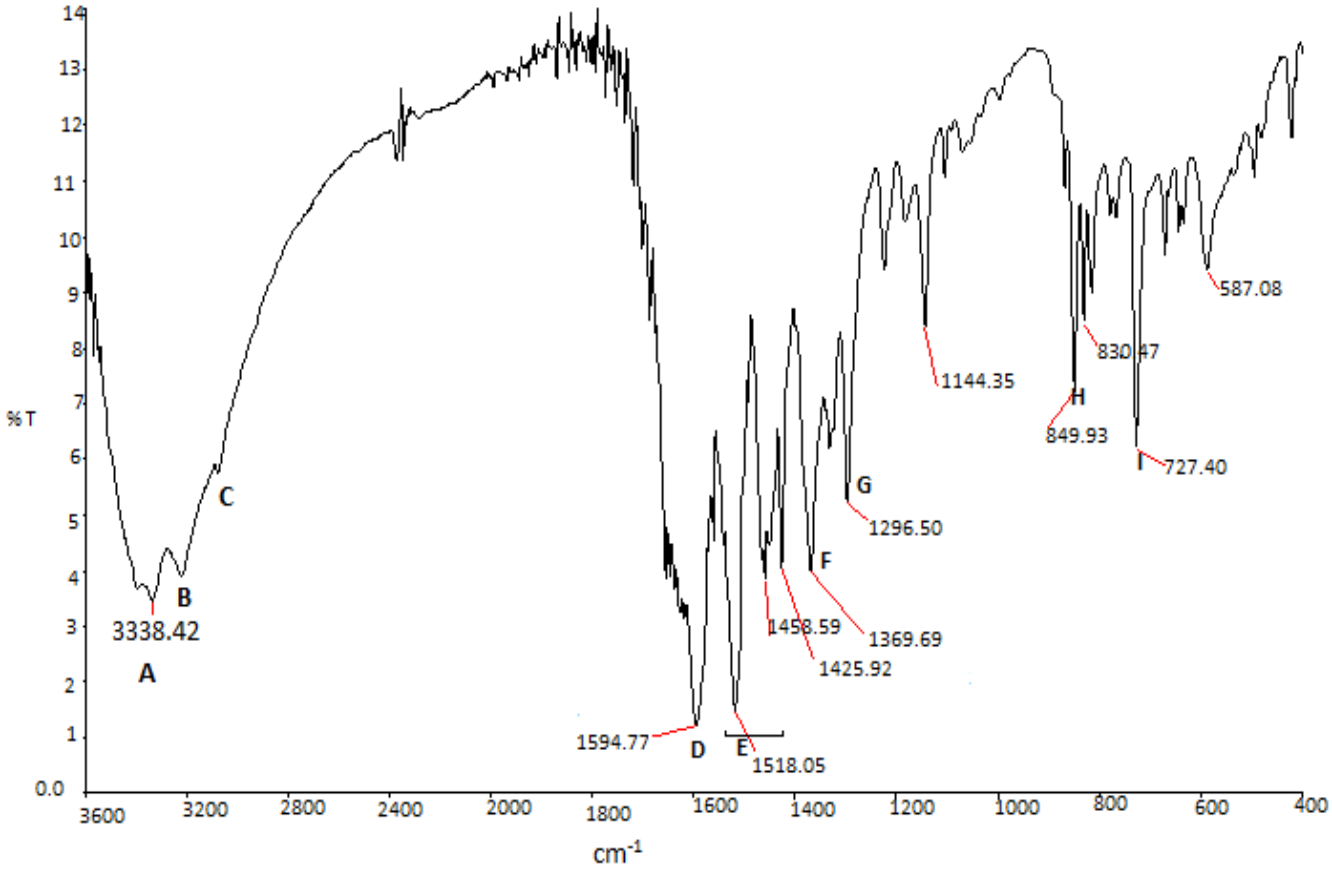

Figure III-7. IR spectra of compound **2** on KBr pellets

A: the ν(NH) vibration of the NH_2(2) group appear at 3338.4 cm^{-1}; hydrogen bonded ν(OH) modes contributes to its broadness;

B&C: the ν(CH) vibration of the phen moiety appear at 3209.5 and 3066.6 cm^{-1} respectively;

D: the $\nu_{as}(CO_2)'$ vibration;

E: ν(C=C), ν(C=N) vibration of the pterin ring;

F: $\nu_s(CO_2')$ vibration;

G: ν(C-O) of pterin phenoxide (4) group;

H&I: the out-of-plane C-H bending vibrations of the phen ring.

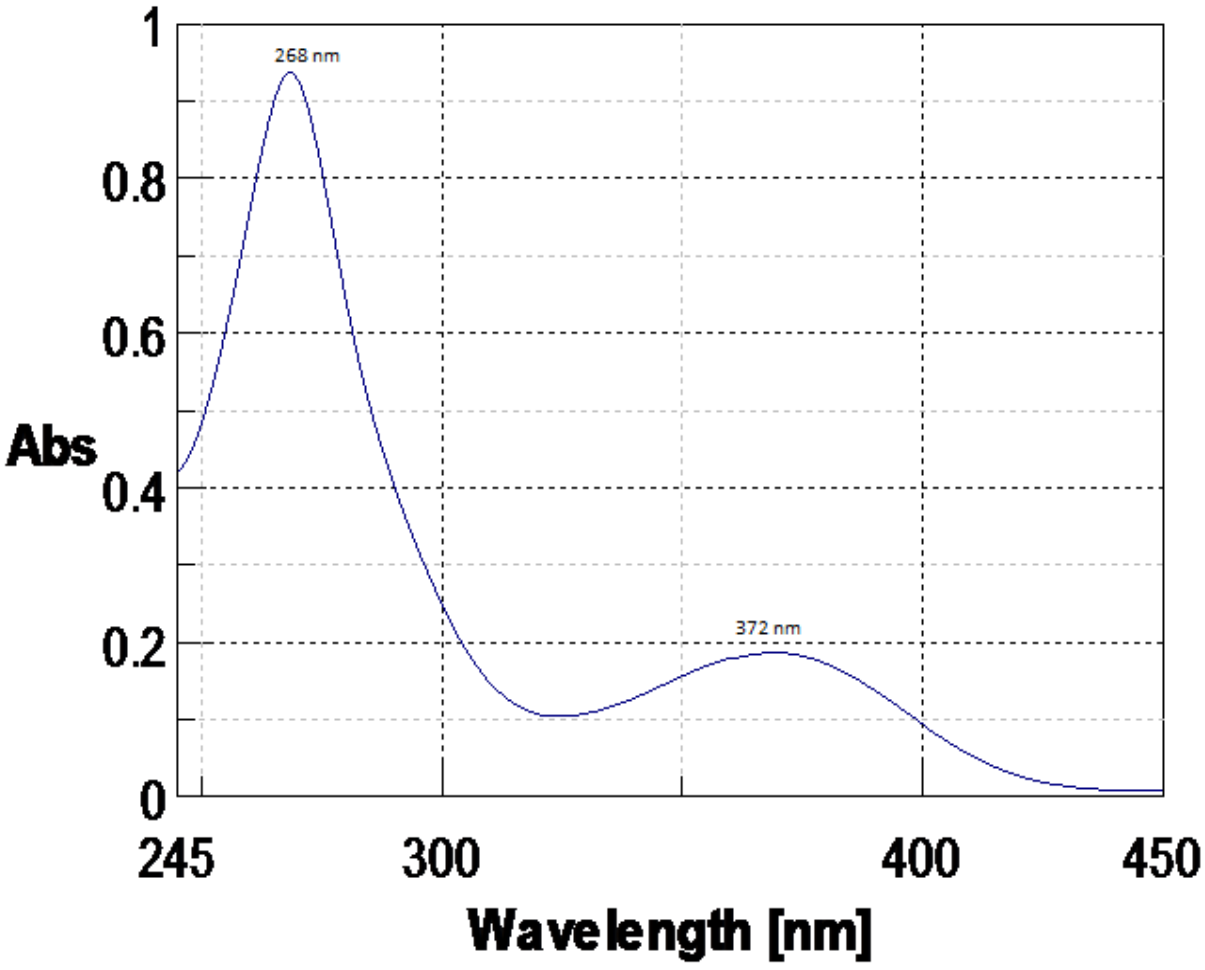

Figure III-8(a). Absorbtion spectrum of **2** in CH_3OH (4.15×10^{-5}M)

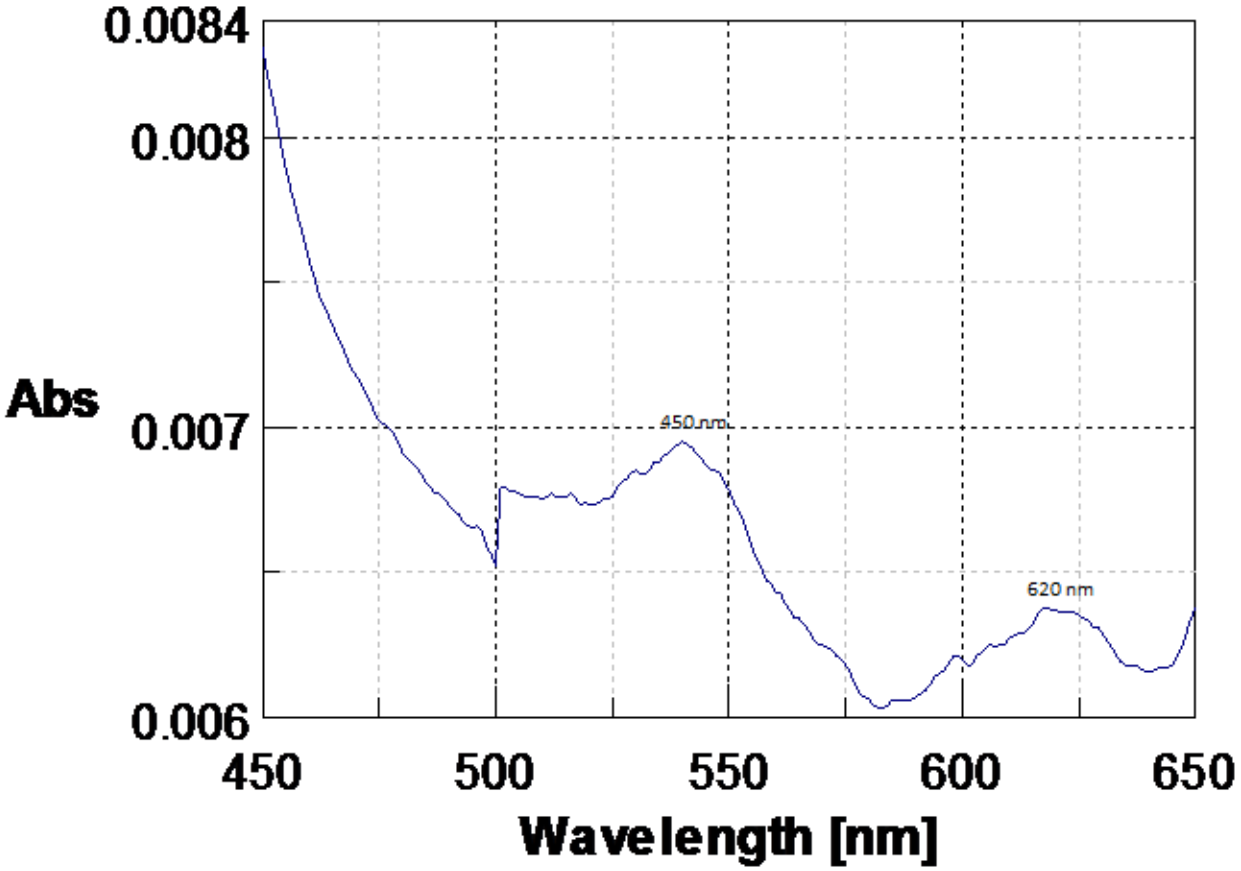

Figure III-8(b).

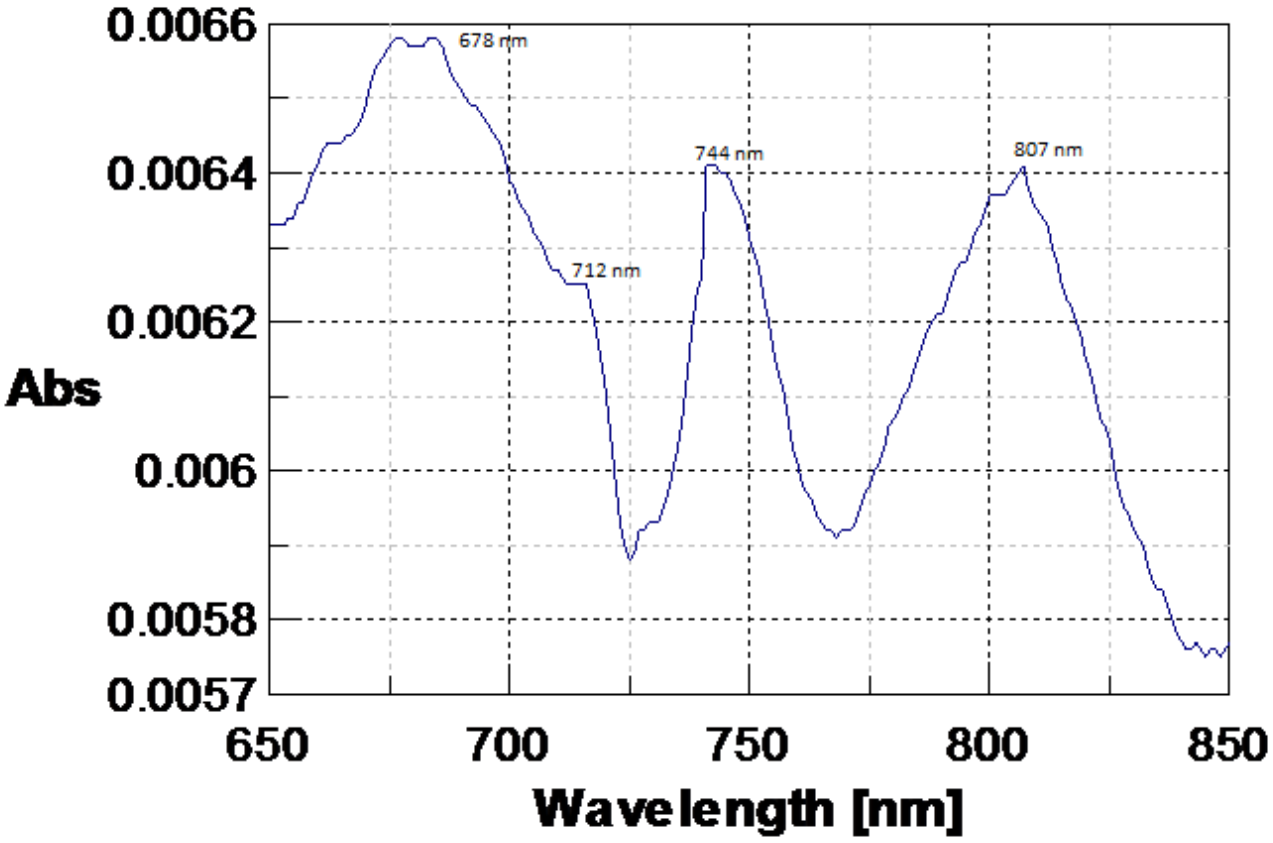

Figure III-8(c).

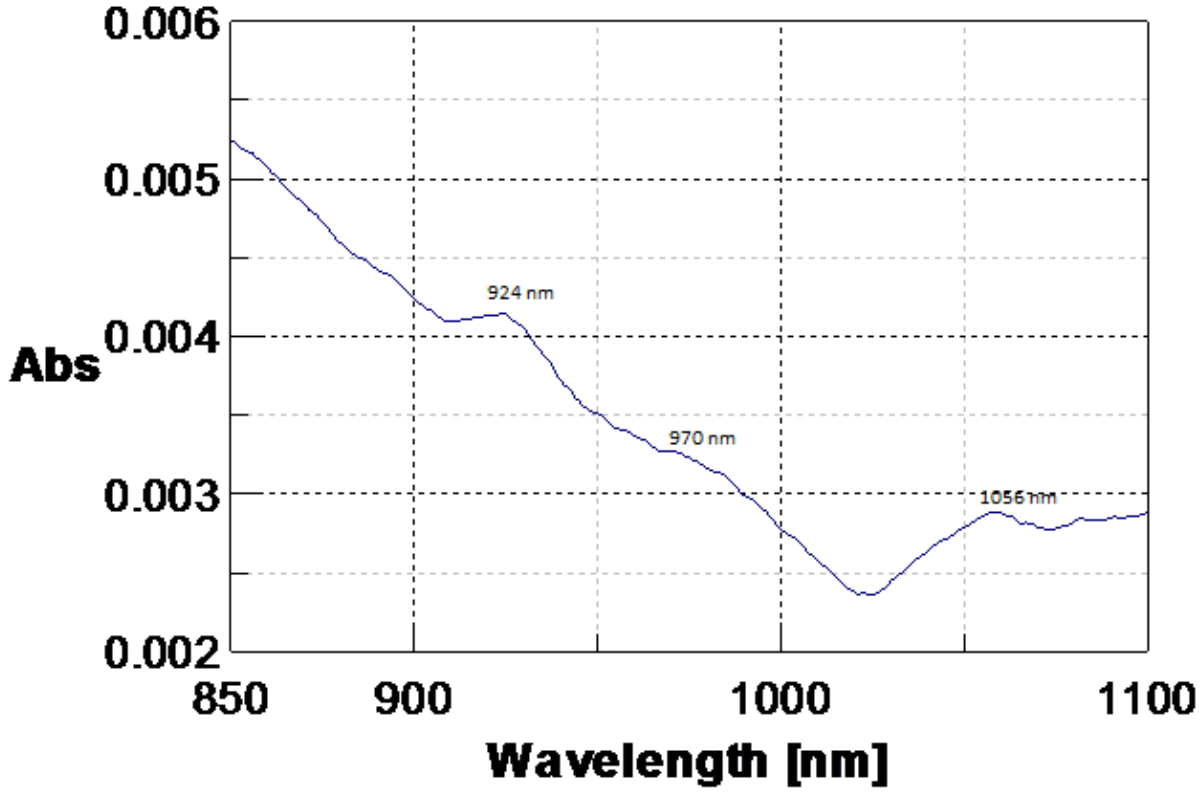

Figure III-8(d).

Table III-4. Electronic spectral data of **2** in CH_3OH

Sl.No.	Compound (solvent)	λ_{max} nm (log ε)

1.	**2**(CH_3OH)	268(4.35), 372(3.65), 540br(2.22), 620br(2.19), 678(2.20), 712sh(2.17), 744(2.18), 807(2.18), 924sh(2.00), 970sh(1.90), 1056br(1.83)

Electronic spectroscopy

The absorption spectral data of compound **2** (orange pink) are summarized in Table III-4 and the relevant absorption spectra in CH_3OH are shown in Figure III-8(a)-(d): Apart from the two prominent bands at 268 nm and 372 nm [Figure III-8(a)] a large number of bands are observed in the longer weavelength region (540-1056 nm) Figure III-8(b)-(d). The intense peak at 268 nm is due to an intra ligand $\pi \rightarrow \pi^*$ transion. The absorption band at 372 nm is assigned to a ligand-to-metal charge transfer transition (LMCT). The relevant lower intensity bands (with ε values in the range 166 – 68) in the longer weave length region may be understood in terms of the following Schemes III- 5 – III-7.

Scheme III-5

Configuration	**Terms (Russell-Saunders states)**
$\mathbf{d^7}$	^4F, ^4P, ^2H, ^2G, ^2F, $^2D(2)$, ^2P

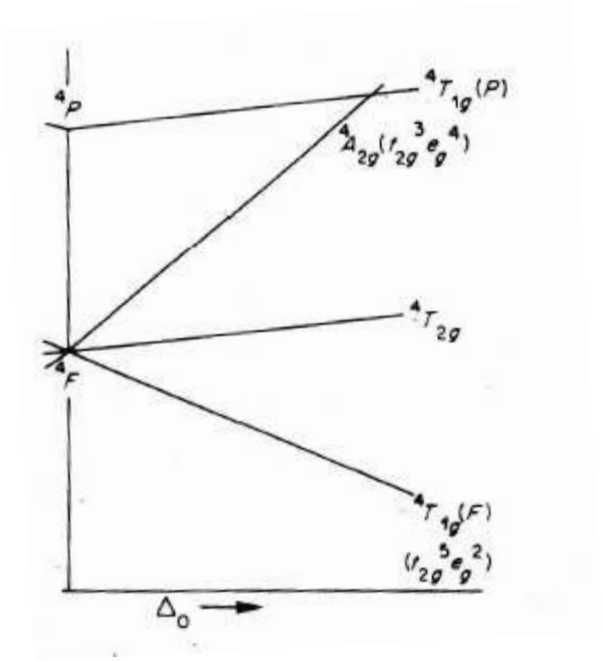

Scheme III-6 Schematic energy level diagram for quartet states of a d^7 ion in octahedral ligand field.[79]

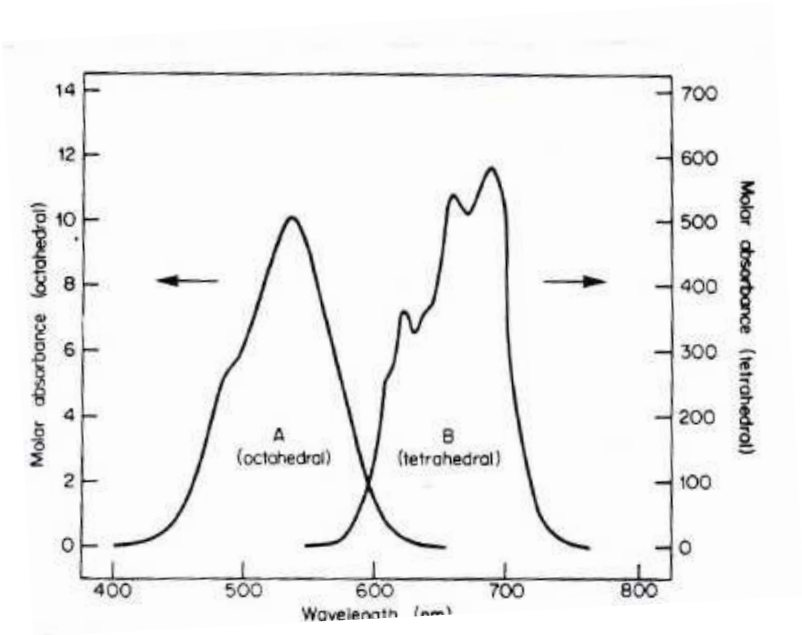

Scheme III-7 The visible spectra of $[Co(H_2O)_6]^{2+}$ (curve A) and $[CoCl_4]^{2-}$ (curve B).[79]

Although in Scheme III-6[79], only the crystal field states in an octahedral field, originating from the quartet states (^4F, ^4P) are shown, there is also possibility of transitions to the higher

dublet states (^{2}H, ^{2}G, $^{2+}$F etc.) shown in Scheme III-5. As the complex **2** lacks a centre of symmetry (Figure III-1), the relevant electronic transitions should be Laporte-allowed/vibronically allowed. The absorption spectrum of $[Co(H_2O)_6]^{2+}$ ion[79] is shown in Scheme III-7; it has a centre of symmetry and the visible region is dominated by the spin-allowed transition $^4T_{1g}(F) \rightarrow {}^4T_{1g}(P)$. For **2** the absorption bands at 540 nm, 620 nm and 678 nm are assigned to the following spin-allowed transitions:-

$$^4T_{1g}\,(F) \rightarrow {}^4T_{2g}(F),$$

$$\rightarrow {}^4T_{1g}(P),$$

$$\rightarrow {}^4A_{ug}(F).$$

The other absorption bands in the longer weave length region (712 – 1056 nm) are assigned to the spin-forbidden transitions to the higher dublet states (originating from the ^{2}H, ^{2}G, etc. states, Scheme III-5). They acquire some intensity through spin-orbit coupling; beside these, they are all Laporte-allowed.

Circular dichroism spectroscopy

The CD spectral response of **2** in CH_3OH is shown in Figure III-9. It reflects several positive cotton effects, e.g. the peak at 307.5 nm is a ligand- based transition, most likely $\pi \rightarrow \pi^*$ transition of the 1, 10- phenanthroline (phen) moiety. The broad CD band centred around 477 nm is due to an optically active ligand field transition associated with the asymmetric/chiral Co(II) center of **2**. Three other weak CD signals could be detected at 679 nm, 779 nm and 823 nm respectively, corresponding to the other different ligand field transitions of **2**. They correspond to some of the electronic spectral data recorded in Table III-4.

The above CD data confirm the absence of a centre of symmetry for **2**, as evident from x-ray structural data as well (Figure III-1).

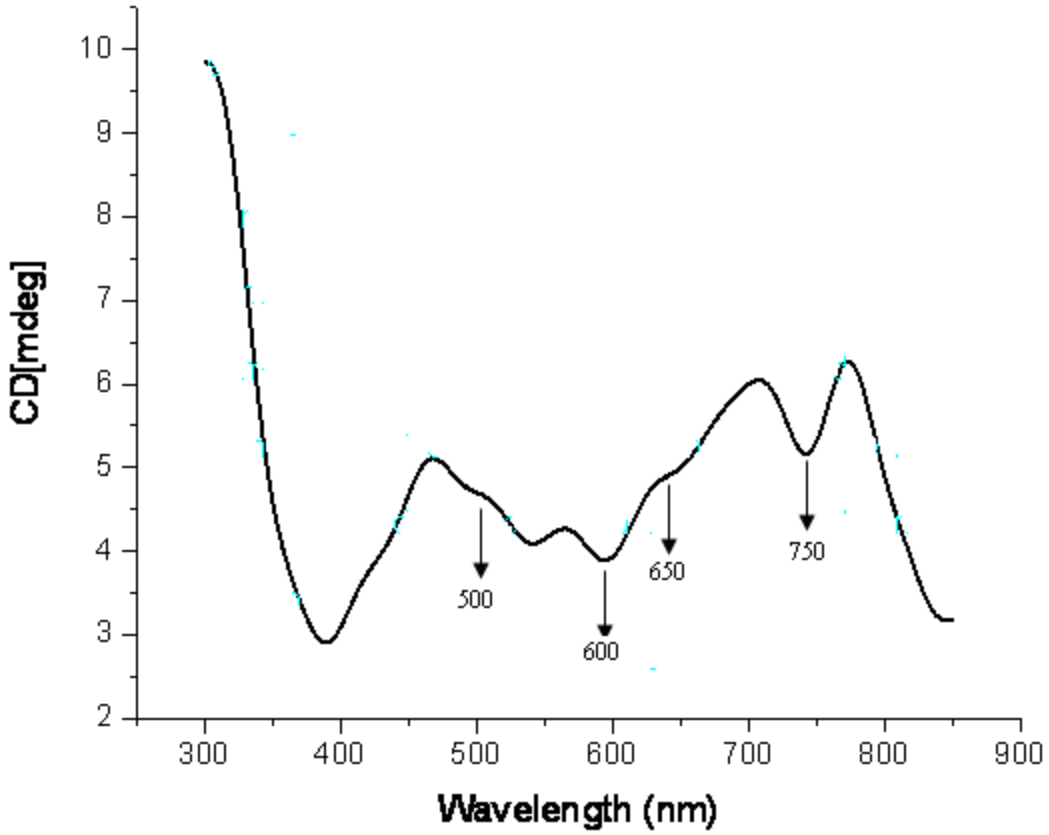

Figure III-9. CD spectral response in CH_3OH of (a) **2 (**($4.7x10^{-4}$M).

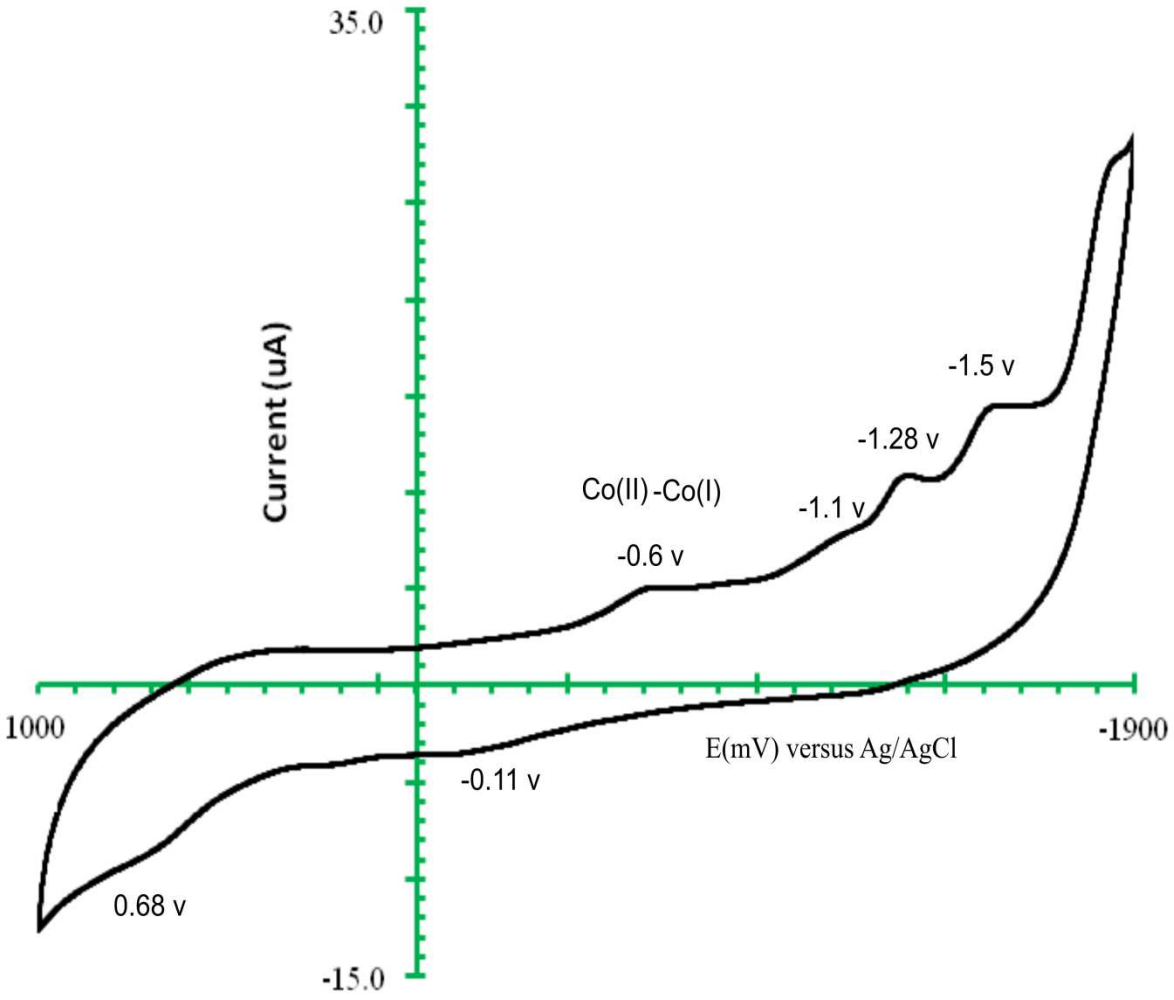

Figure III-10. Cyclic voltammetry data of **2** in DMSO (0.1mM; 0.1M TBAP; GCE) at a scan rate, 100 mVs^{-1}; the potential scan starts from – 1900 mV and terminates here.

Cyclic voltammetric studies

Cyclic voltammetric data of **2** is shown in Figure III-10. The present ligand (**1**) characterized by a single irreversible reduction peak (E_{PC}) at -418 mV (ca. $1x10^{-3}$ mol dm^{-3} in aquous NaOH medium, pH ca. 10 with 0.1M dm^{-3} KNO_3; scan rate, 100 mV s^{-1}). Figure III-10 shows several irreversible reduction as well as reoxidation steps. The peak at -0.6 v is a metal-centred process, reflecting the reduction Co(II)→Co(I). In terms of the frontier orbitals of **2** (Figure III-17), the LUMO and LUMO +1 levels are characterized by a small band gap (0.03 eV) and making this reduction step feasible. Actually, the Co(I), d^8 state is characterized by several well-defined compounds with π-acid type ligands like CO, 2,2-bipyridile, etc.[79] Besides this, the Frost diagram for the cobalt system over the oxidation states +2 and +1 is quite flat, almost parallel to the x-axis i.e. a small change in free energy ($\Delta G^0 \infty$ NE˚/V) can achive interconversion between the two oxidation states.[80] As evident from the irreversible nature of this reduction (Figure III-10), the present ligand environment (phen and pterin) is unable to cope with the change associated with the above electron transfer, leading to decomposition of the reduced complex through solvent attack. The corresponding bipy-containing complex, [Co(L)(bipy)(H_2O)]. $3H_2O$ (chapter VI) shows a quasi-reversible behavior (Figure VI- 27) because of the better adaptability of bipy ligand to the present situation.[79]

Figure III-10 indicates three ligand-centered reductions of **2** at -1.1V, -1.2V and -1.5V respectively. Besides these, two reoxidation peaks appear at -0.11V and 0.68V respectively. At least some of the above-mentioned metal-and ligand-centred reductions of **2**, could be achived on a preparative/scale by treating it with $NaBH_4$ in CH_3OHmedium and the resulting compound **3** coould be isolated in the solid state (vide the experimental section).

Fluorescence emission spectra. The fluorescence emission spectra of **2** and **3** in CH3OH are shown in Figure III-11; their emission maxima appear at 450 nm and 455 nm respectively. Such emission maximum of the pterin ligand (**1**) (in aqueous NaOH solution) appears at 449 nm (Figure II-10).

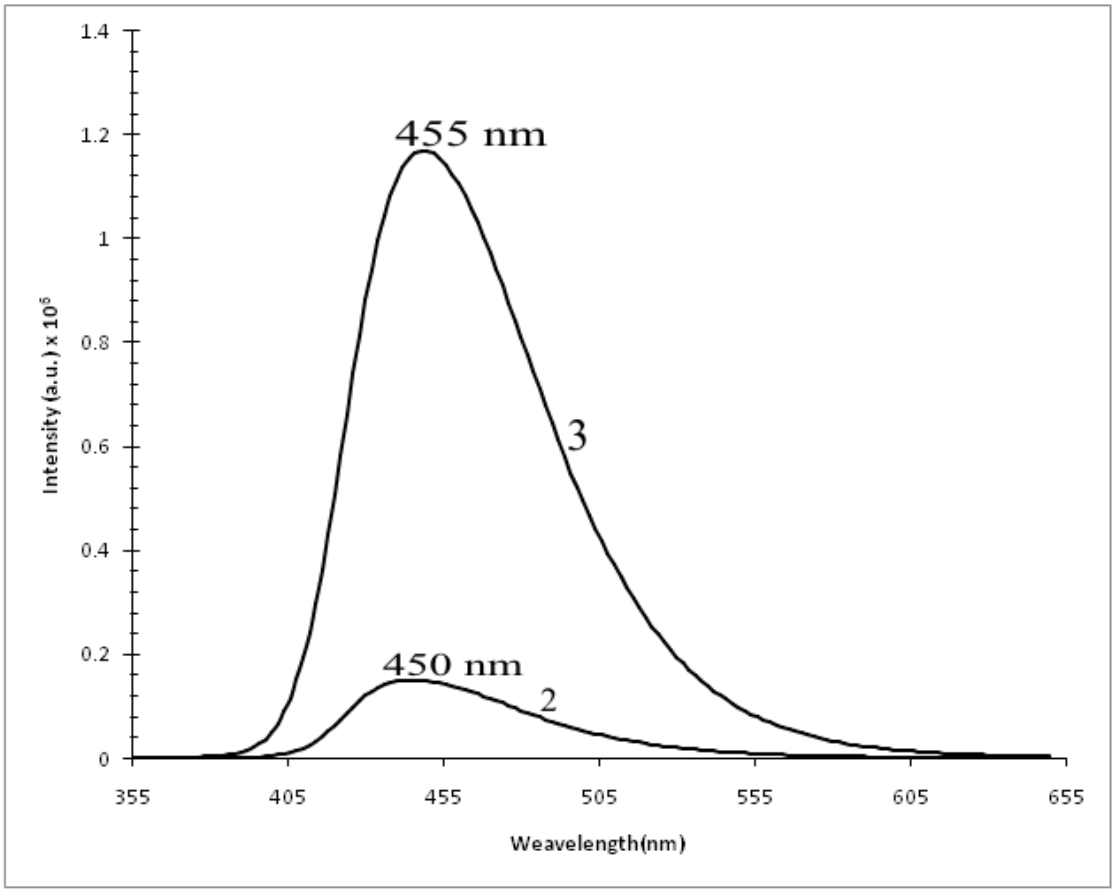

Figure III-11. Fluorescence emission spectra of **2**(CH_3OH, 1.4 x 10^{-4} M), **3** (CH_3OH, 4.6 x 10^{-5} M).

In terms of the intensity scale (a.u.) there is a drop in fluorescence intensity on complex formation process [H_2L(**1**) → **2**], but on reduction with $NaBH_4$ [**2** → **3**] there is a considerable increase in intensity. This modification of intensity values (au) can be related to the change in electron density on the pterin ligand center as well as the metal center, during the above transformations [**1** → **2** → **3**].

Fluorescence data constitute an important property of pterin compounds, e.g., such data provided with the initial evidence about the pterin component of the molybdenum cofactor.[33 - 34] The pH dependence of fluorescence property is also interesting, e.g., no fluorescence is observed for the protonated form of biopterin but the anion is strongly fluorescent.[35] Most organic fluorescent molecules contain conjugated system of double bonds with extended π-orbitals in a planar cyclic/rigid structure and not many loosely coupled substituents through which the vibronic energy can dissipate.[36] The common fluorophores include aromatic / heteroaromatic rings as well as functional groups like C = C, C = O , C =N, etc., while fluorochromes (usually electron donors) like – OH, - NH_2, etc., enhance the transition probability or fluorescence intensity. The enhanced fluorescence intensity of **3** (Figure III-11) which is obtained by the $NaBH_4$ reduction of **2** in CH_3OH, may be understood in the light of greater electronic circulation in **3** due to Co(I)(d^7) → phen type charge transfer transition ;[32] the reduced pterin ring (7,8-dihydro form) also assists this process.

Reactivity of 2

As evident from the molecular structure of **2** (Figure III-1), it possesses an aquo group as well as two redox centers, e.g., the Co(II) atom and the redox non-innocent pterin ligand residue.

Its reactivity towards suitable reagents have been studied for exploring the group transfer (aquo group) and redox reactivities.

Reactivity with imidazole

Figure III-12 represents the absorption spectral changes associated with the reaction of **2** with imidazole in CH_3OH at 328K. Imidazole is related to the histidine residue of many protein chains and is well-known for its affinity towards the first transition metals in the biological systems. Kinetics of this reaction was followed at 372 nm and four different temparatures in the range 308-328K under psudo-first order conditions (approx. 100 times excess of imidazole ligand). Observed rate constants were determined by least square method from the plots of $\log(A_t-A_\infty)$ versus time, which were linear for three half-life.[49,50.] The relevant data are as below:

$k_{obs} = 2.6 \times 10^{-2}\ s^{-1}$; $\Delta S^{\neq} = -256.0\ J\ mol^{-1}\ deg^{-1}$.

They are consistent with a ligand substitution process (Scheme III-8) through an associative path way.

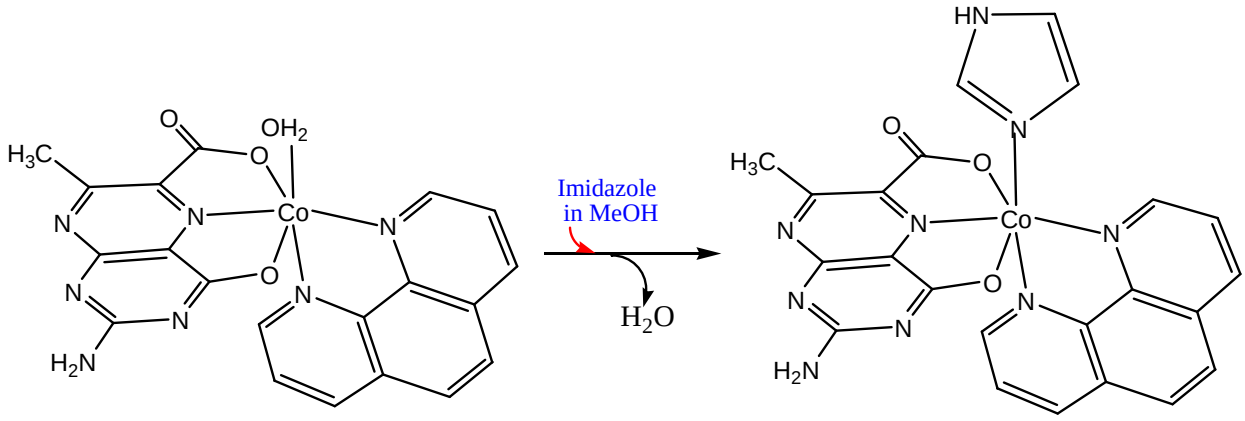

Scheme III-8

Scheme III-8 summarizes the above reactivity, indicating the formation of a imidazole substituted compound. Stoichiometry of the above process could be established x-ray crystallographically for the corresponding Ni(II) system containing an imidazole ligand in its coordination sphere.[17c]

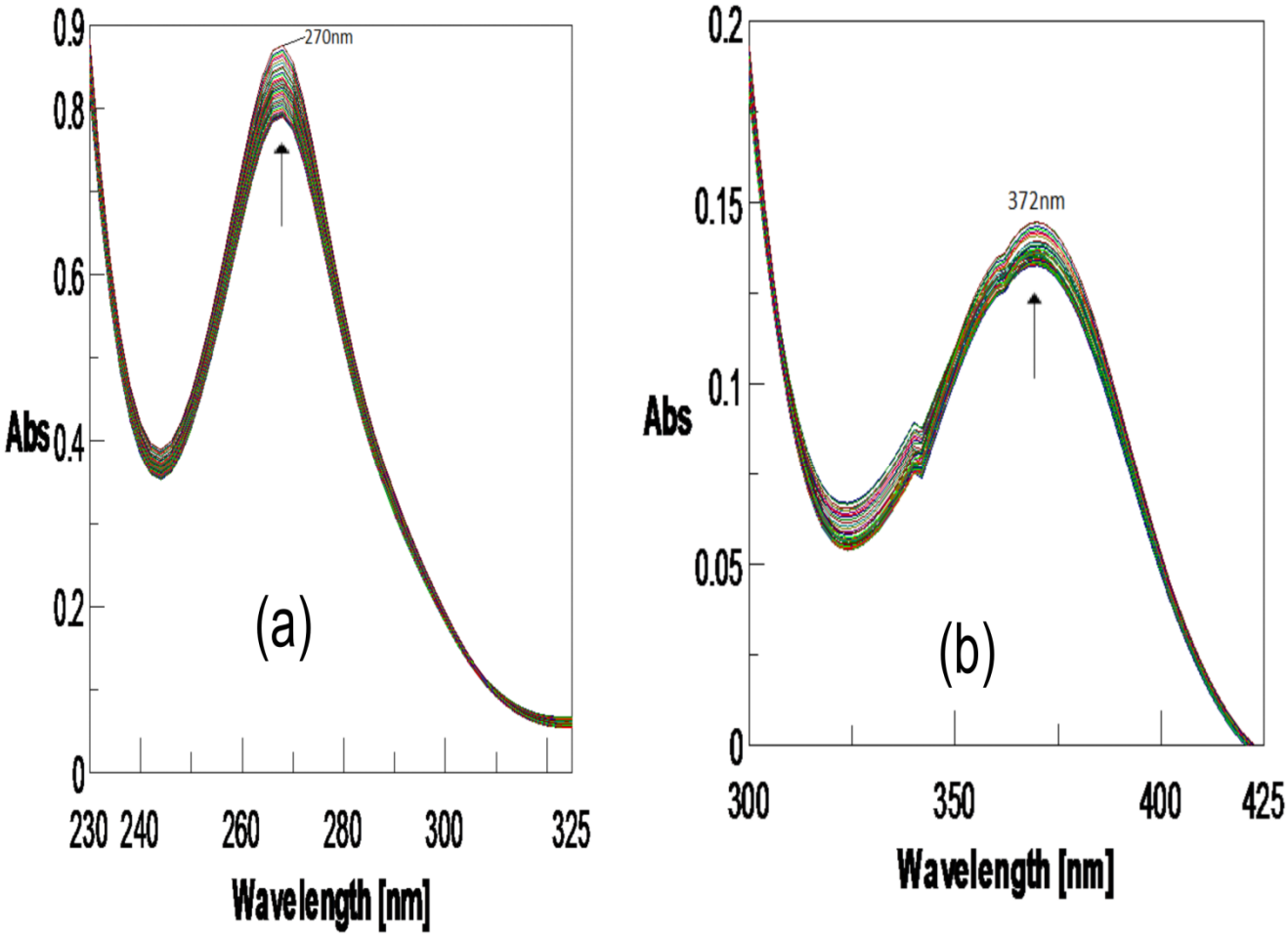

Figure III-12. Absorption spectral changes recorded at 6 minute interval during the reaction of **2** (1.42 x10^{-5} M) with imidazole (Im) (3.6 x10^{-2}M) in CH_3OH at 328K; (a) over the range 230- 325 nm; (b) over the range 300-425 nm.

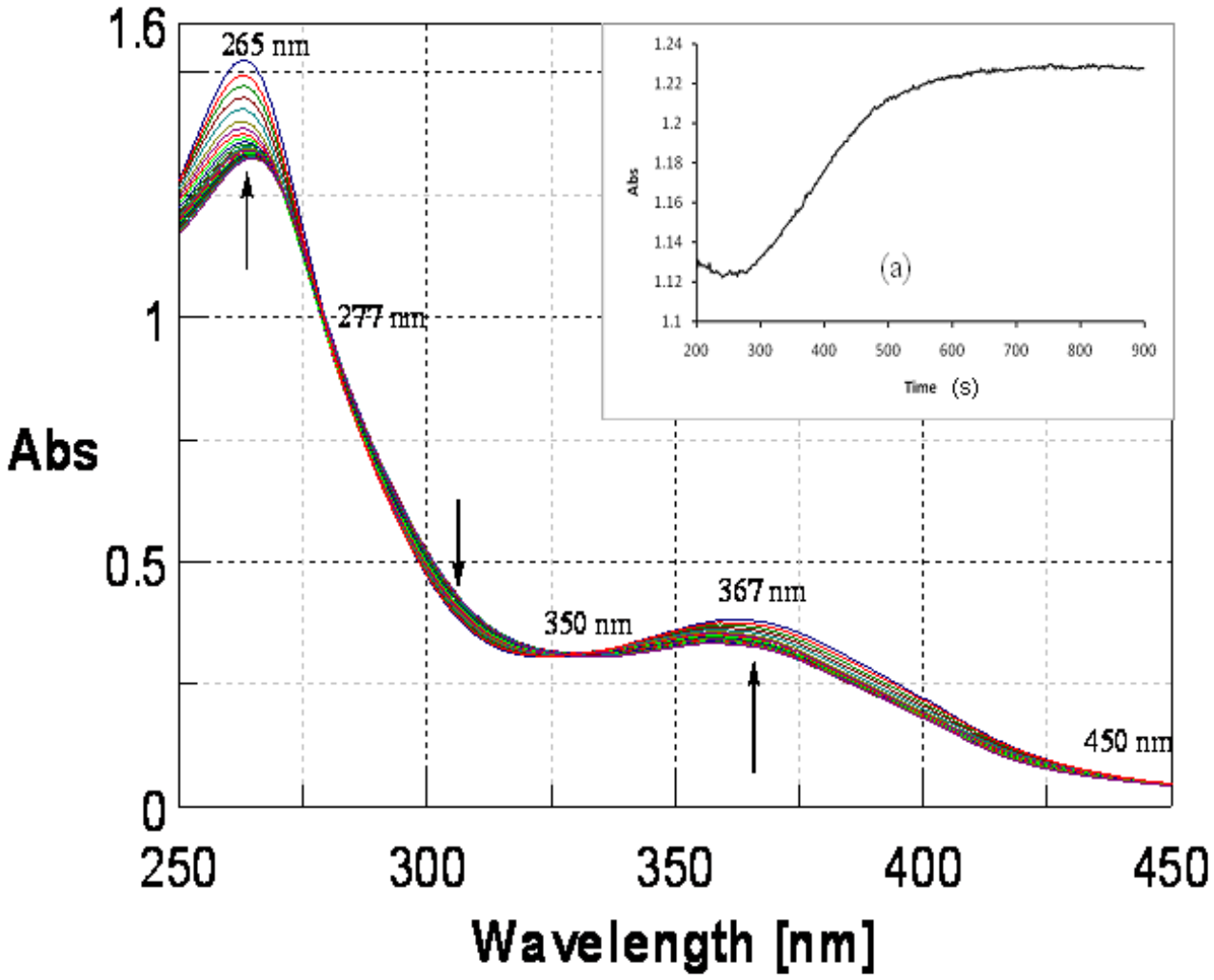

Figure III-13. Absorption spectral changes recorded at 2 min interval during the reaction of **2** (8.9×10^{-5}M) with $NaBH_4$ (6.9×10^{-2}M) in CH_3OH at 298K showing three isosbestic points (at 277, 350 and 450 nm).The inset (a) shows the kinetic trace at 367 nm.

Reactivity of 2 towards sodium borohydride ($NaBH_4$)

It is worthwhile to explore the reactivity of **2** towards $NaBH_4$ to find out its ability of accepting reducing equivalents at both the metal and pterin ligand centers (Figure III-13). Literature data indicate an E°′ value of -0.75 V for $NaBH_4$ in neutral medium.[56-58] In terms of the cyclic voltammetry data of **2** (Figure III-10), the metal center [Co(II)] and at least the pyrazine ring of the pterin ligand residue, should be susceptible to $NaBH_4$ reduction. Figure III-13 shows the absorption spectral changes recorded during the reaction of **2** with $NaBH_4$ in CH_3OH at 298K. Distinct changes in absorbance values are observed at 265 nm and 367 nm respectively, affecting both the ligand-centered ($\pi \rightarrow \pi^*$ type) and metal-centered (LMCT type) transition regions. The presence of isosbestic points at 277 nm, 350 nm and 450 nm respectively, indicate a clean conversion (reduction) during reaction with $NaBH_4$, without major structural change. Kinetics of this reaction with $NaBH_4$, was followed at 367 nm and four different temperatures in the range 300-330K in CH_3OH under psudo-first order condition (with a **2** : $NaBH_4$ ratio of 1 :140). The following kinetic parameters were evaluated:

$k_{obs} = 2.68 \times 10^{-3}\ s^{-1}$; $\Delta S^{\neq} = -198.0\ J\ mol^{-1}\ deg^{-1}$.

The above results point towards a group transfer reaction involving an associative step. Stoichiometric study of this reaction was carried out by isolating the relevant reduction product **3**, as already discussed under the heading of experimental section, cyclic voltammetry and fluroscence spectroscopy.

Scheme III-9 shows the reaction between **2** and $NaBH_4$, leading to the formation of the 7, 8-dihydro form of the pterin ligand and the reduction of the metal center [Co(II) → Co(I)] in **3**, in conformity with the cyclic voltammetry data of **2** (Figure III-10). Of the different possible dihydro forms of pterin, 7, 8- dihydro form is the most stable one [10] due to overall planarity of

this partly reduced pterin ring, as verified x-ray structurally by Viscontini and coworkers.[81] The fluorescence spectral

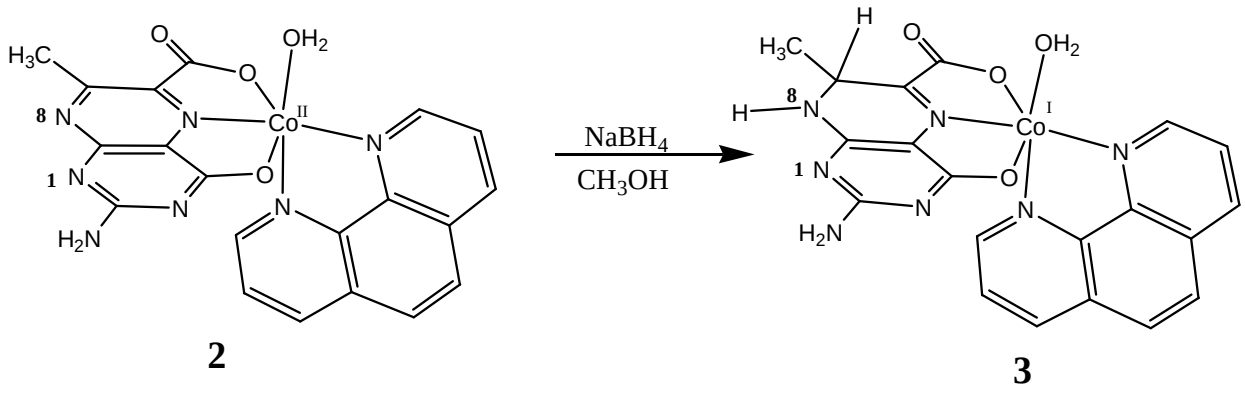

Scheme III-9.

---

data (Figure III-11) reflect this increase in electron density in the pterin ring. Besides this, the steric/stereo-electronic factors of the ligand environment of **3**, helps to assimilate these reducing equivalents from $NaBH_4$ without much structural rearrangement.

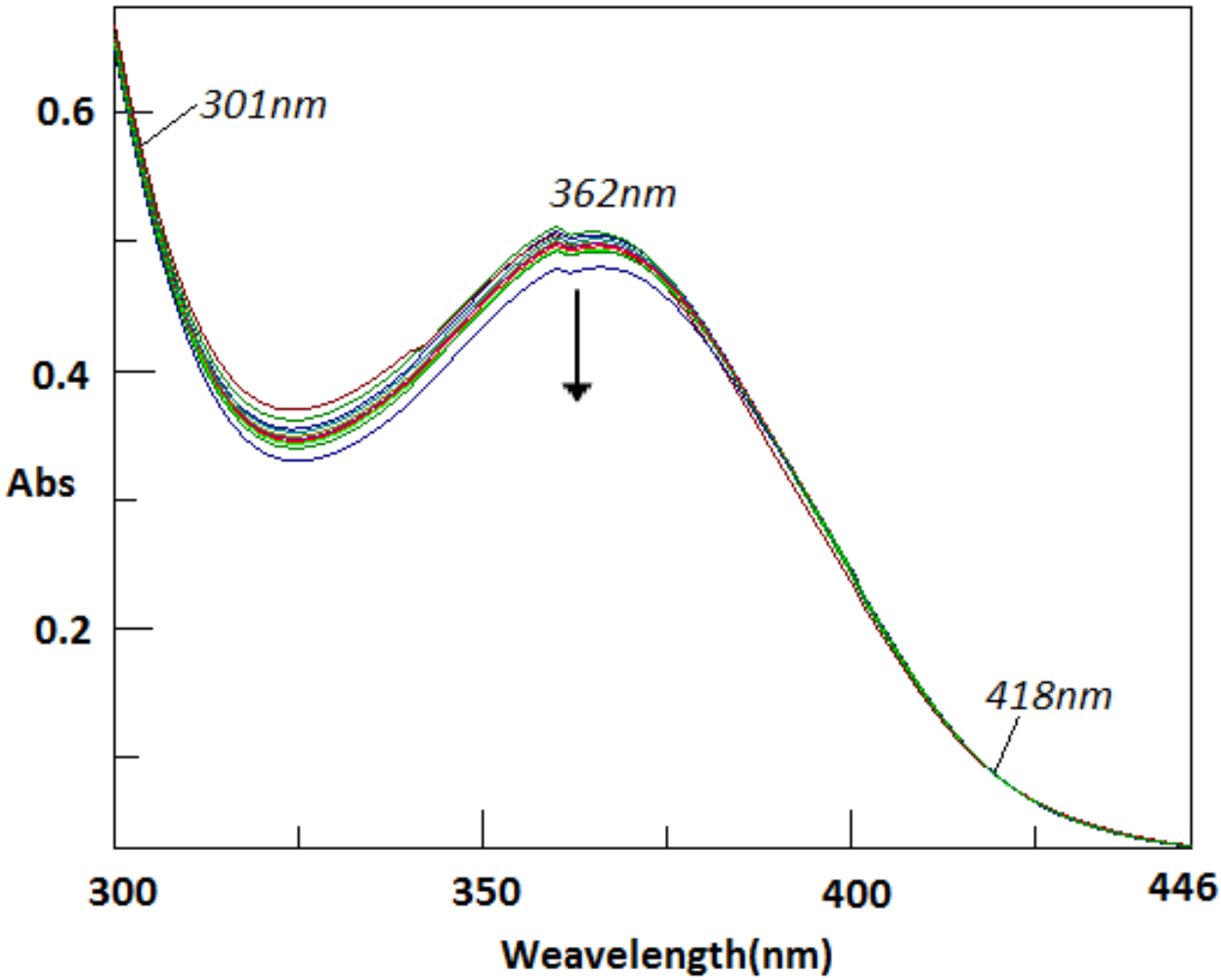

Figure III-14. Absorption spectral changes recorded at 5 min interval during the reaction of **3** (1.0×10^{-4}M) with bromobenzene (1.9×10^{-2}M) in CH_3OH saturated with O_2 at 300K.

Reactivity of 3 with bromobenzene (model substrate) in presence of O_2

Figure III-14 explores the reactivity of the $NaBH_4$ reduced compound **3** with bromobenzene in presence of dioxygen in CH_3OH. A distinct change in absorbance values occur at 362 nm (LMCT region) with a clean isosbestic point at 418 nm and a close approach to such an attribute at 301 nm. Nature of such changes is opposite to that in Figure III-13. Kinetics of this reaction (Figure III-14) was followed at 362 nm and foure different temparatures (range 300-330K) in CH_3OH saturated with O_2 under psudo-first order conditions (with a **3**: bromobenzene ratio of 1 : 140) and the relevant data are indicated below:

k_{obs} =2.86 x 10^{-2} s^{-1} ; $\Delta S^{\neq}$ = -186.0 J mol^{-1} deg^{-1}.

In terms of k_{obs} values, the transfer of reducing equivalent from **3** to bromobenzene is approximately 10 times faster than the transfer of reducing equivalent from $NaBH_4$ to **2**. Figure III-15 and III-16 show the reactivity of $NaBH_4$ in CH_3OH medium with 1, 10-phenanthroline and the pterin ligand **1** respectively. While 1, 10-phenanthroline remains essentially unaffected over the relevant spectral region (362 nm), the

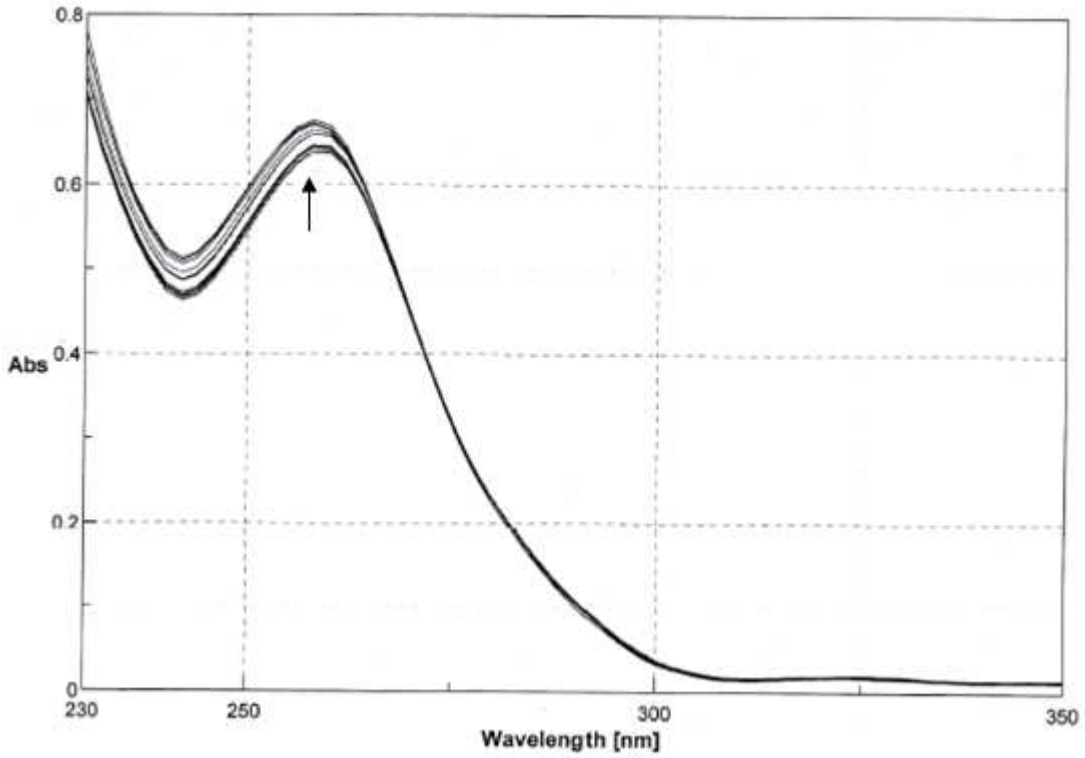

Figure III-15. Absorption spectral changes recorded at 2 min interval during the reaction of 1, 10-phenanthroline monohydrate (phen) (1.25×10^{-3}M) in CH_3OH at 303K with $NaBH_4$ (1.35×10^{-2}M).

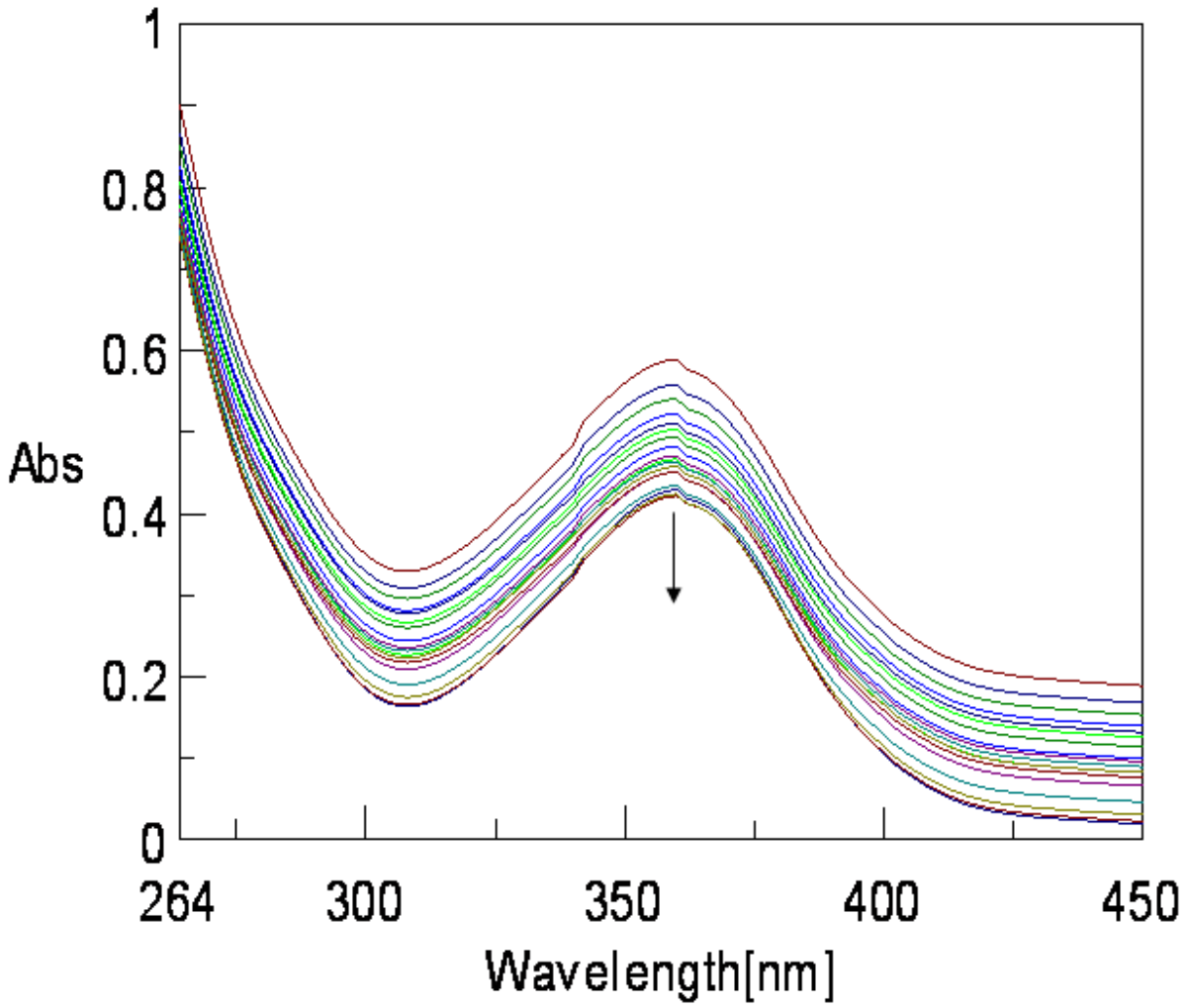

Figure III-16. absorption spectral changes recorded at 2 min interval during the reaction of **1** (1.34 x10^{-3} M) in aqueous NaOH solution (1.25 x10^{-2} M) with $NaBH_4$ (1.35 x10^{-2} M) at 303K.

---

pterin ligand undergoes reduction over same spectral region. This indicates that the pterin ligand is the reaction locant of **2** during reaction with $NaBH_4$ (Figure III-13).[22, 23] However, the nature of the absorption spectral change in Figure III-16 is different (absence of isosbestic points) from

those in Figure III-13, indicating considerable modification of the pterin ligand moiety through complex formation with the Co(II) center in **2**.

In view of the reactivity data as evident from the above discussions on Figure III-13 to Figure III-16, **2** serves as an excellent mediator of reducing equivalents from $NaBH_4$ to bromobenzene in presence of dioxygen (O_2), leading to the formation of 4-bromophenol; this aspect has been verified from reaction stoichiometric studies as outlined in chapter II. Mechanistic details of this process are outlined in the next section.

Electronic structure of 2

The electronic structure of **2** was obtained by DFT calculations, performed using the Gaussian 09 package. Molecular orbitals were visualized using " Gauss View 5.0" . The method used was B3LYP hybrid-exchange functional and 6-31g basis set; the x-ray refined structure parameters were use as the input parameters. Since the x-ray refined structure parameters were used, optimization of the structure was not carried out here and the ground state energy minimization calculation gives the frontier orbitals diagram as shown in the Figure III-17. along with their energies and the compositions (%). The most remarkable aspect of Figure III-17 is the small band gap (0.3 – 0.5 eV) between the adjacent levels of the frontier orbitals, which is as low as 0.03 eV between the LUMO and LUMO+1 levels. The molecules with low HOMO/LUMO gaps are of particular importance due to their ability to easily donate (from HOMO) or accept (on LUMO) an electron, which is the basic process in all organic electronic devices. From chemical point of view such molecules can posses electrochemical/redox amphoteric behavior due to low barrier to thermo-excited electron transfer in either direction.[82] The present electrochemical and redox reactivities of **2** , as presented in Figure III-10, III-11, III-13, III-14 throw light on this

aspect . For example, cyclic voltametric data of **2** can be interpreted on the basis of reduction of both the metal and pterin ligand centers as well as reoxidation of the reduced pterin ligand. Again , the reaction of **2** with $NaBH_4$ and further reaction of the reduced complex **3** with bromobenzene/O_2 mixture, involves input of electron density into the LUMO/LUMO+1 levels as well as transfer of reducing equivalents out of them.

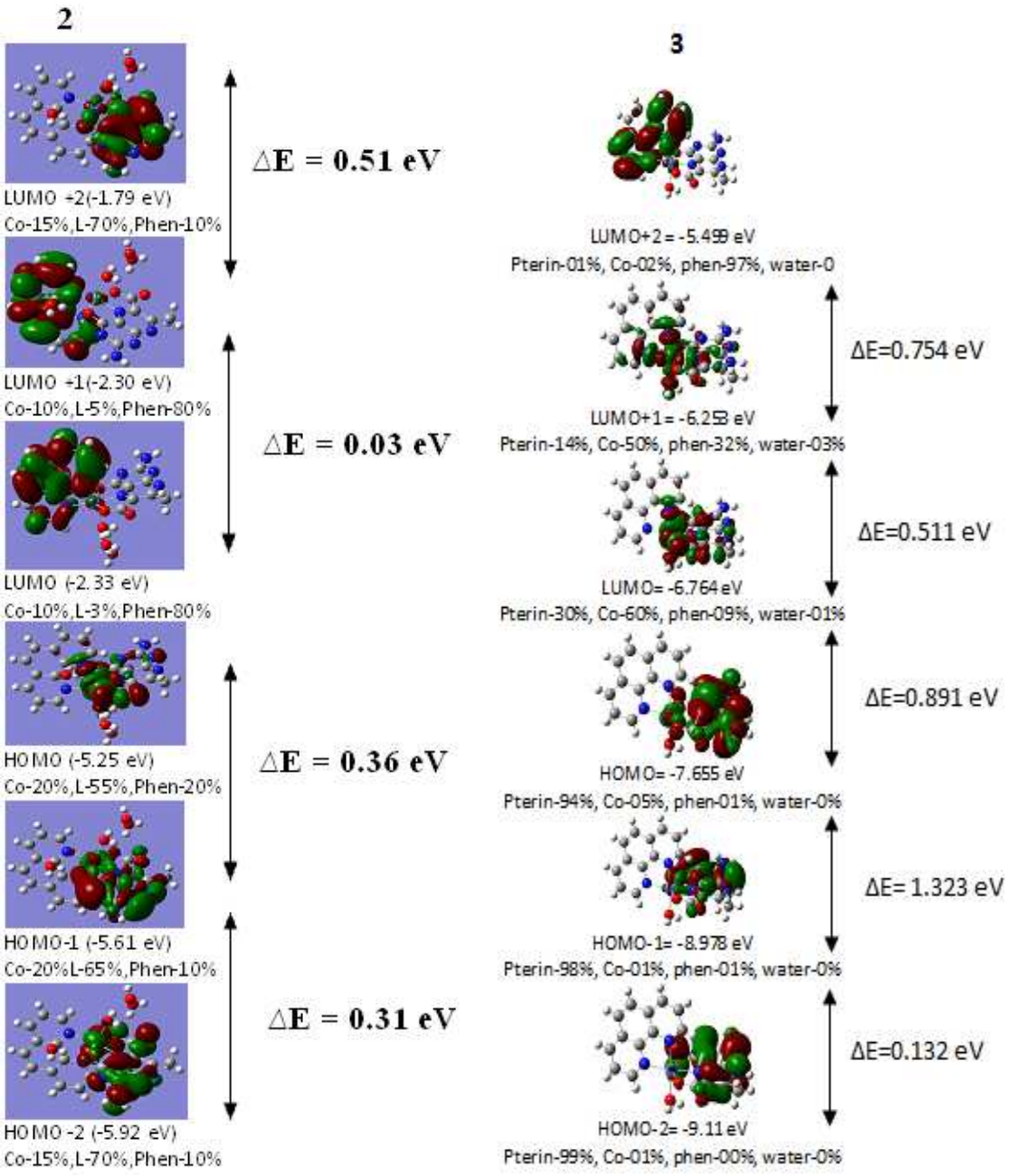

Figure III-17. Frontier molecular orbitals of **2** and **3**, showing their energies (eV) and compositions (%).

This redox amphoteric behavior of **2** is the high light of this work and it correlates well with the above-mentioned low energy band gaps (Figure III-17). Besides this, the compositions (%) of the

HOMO/LUMO levels give some hint regarding the nature of the electron transfer involved here. In this region, percentage contribution of the Co(II) center changes from 20% → 10%; the pterin ligand contribution changes over the region 55% → 3/5%, whereas phen contribution varies from 20 % → 80%. Thus the difference between the LUMO and LUMO+1 level, is controlled by a change over in pterin contribution from 3% →5%. In practical terms, LUMO and LUMO+1 levels are almost identical in terms of energies and compositions.

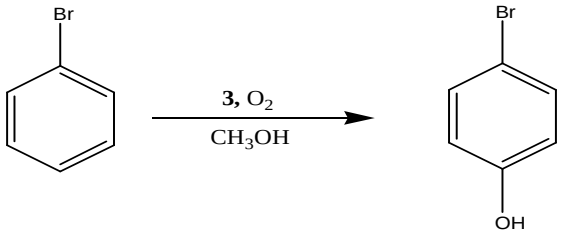

Scheme III-10

Electrophilic oxygen addition to the substrate,RH

Monooxygenase type activity of **3** using O_2 as the source of oxygen atom transferred:

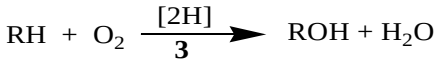

[2H]: reducing equivalents transferred by **3**

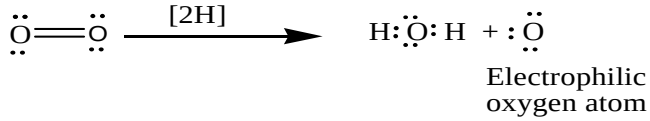

Scheme III-11

This aspects helps to rationalize the reactivity of **2** as shown in Scheme III-9. Oviously, the reduced complex **3** is of leaser stability and is correctly poised to react with the bromobenzene/O_2 reaction system (Scheme III-10). The reducing equivalents stored in **3** play a

decisive role in activating the dioxygen molecule (O_2), producing the incipient electrophilic oxygen atom (Scheme III-11), which is transferred to the substrate RH, producing ROH, in other words, this is the basis of monooxygenase type activity of **3**.[100,101]

Conclution

This chapter presents the synthesis, characterization and reactivity aspects of a new mixed ligand Co(II) complex. Its spectroscopic, cyclic voltammetric and redox reactivity data could be rationalized in terms of the electronic structure (DFT) as well as the Frost diagram. The corresponding $NaBH_4$ reduced complex **3** could be characterized to be a Co(I) species, a rare event in pterin chemistry. During its reaction with the bromobenzene/O_2 reaction mixture, most likely a Co(I)→O_2 electron transfer step activates the dioxygen molecule;[99] Scheme III-12 shows the possible pathway through MO formation,[30,31,90,102] through replacement of the aquo group from the z-axis by O_2 (Scheme III-9). Finally, the reduced pterin ring of **3** (Schemes III-9, to III-11) completes the process of reduction of one of the oxygen atoms to the level of water and the other oxygen atom is incorporated into the substrate (bromobenzene), thereby completing the monooxygenase type activity.

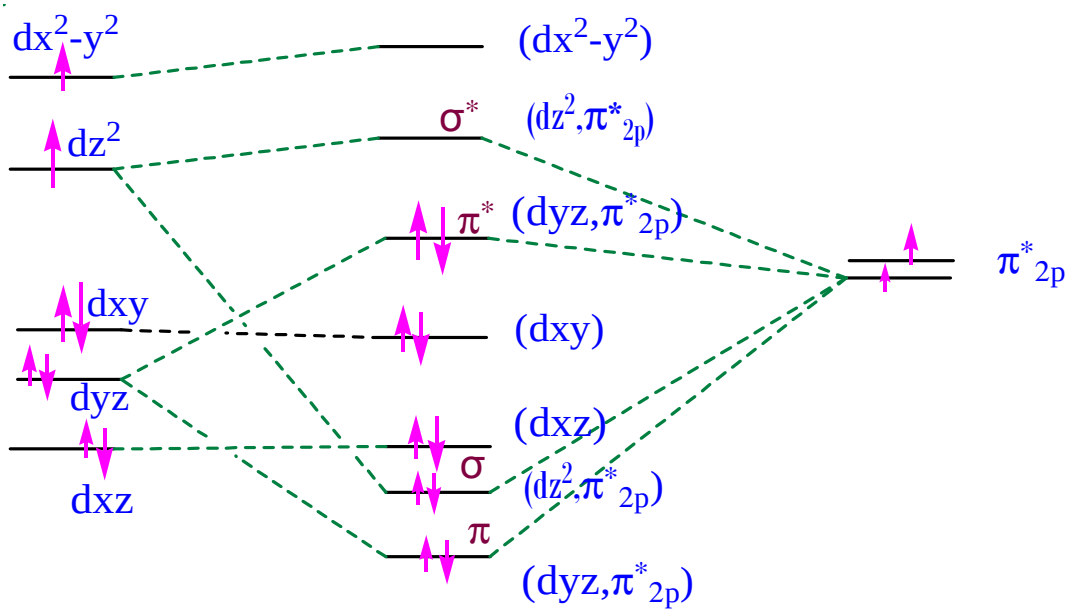

3 **3**(O_2)Complex : a O_2 Hypothetical intermediate step involved in Scheme III-10 & III-11

Scheme III-12 This MO picture is based on Scheme III-9 whereby the aquo group of **3** is replaced by O_2 along the Z-axis as well as participation from the dz^2 (σ-type) and dyz(π-type) orbitals. The other d orbitals (d_{xz}, d_{xy} and $d_{x^2-y^2}$) remain nonbonding.

This model monooxygenase type activity is the result of joint participation by both the redox active metal centre and the redox non-innocent pterin ligand centre of **2**.[10,52-55,99-101]